THOMAS DØSSING

General Survey of Heavy Ion Reactions and Specific Problems in Damped Nuclear Reactions

ABSTRACT. *A general introduction to heavy ion reactions is given, consisting of a brief survey of the whole bombarding energy spectrum, from damped nuclear reactions to ultrarelativistic collisions, followed by a short review of theories of damped nuclear reactions. A more specialized discussion is made for the angular momentum dynamics in damped nuclear reactions, studied with the nucleon exchange transport theory. The theory is applied to study the polarisation of γ rays emitted in the sequential decay of the reaction products, and to Wilszinsky plots. The results for these quantities compare well to data for energy losses less than half of the maximal energy loss, but the predicted fluctuations in energy loss and scattering angle are too small to account for the data at larger energy losses.*

The Niels Bohr Institute, Blegdamsvej 17,
DK-2100 København Ø, Denmark

1. Introduction

Deep inelastic collisions between atomic nuclei, or, as we shall prefer to call them, damped nuclear reactions, were first observed in 1961. Since the application of more powerful accelerators and more refined detectors around 1975, a more intense study of these reactions has been carried out, both experimentally and theoretically.

A damped nuclear reaction typically proceeds as follows. A heavy projectile nucleus with a kinetic energy of several MeV per nucleon is bombarded onto a heavy target nucleus. The two nuclei engage in a reaction during which a substantial part of the available energy is lost from the relative motion. Still, the emerging nuclei after the reaction resemble the original ones with respect to their mass and charge numbers. This approximate preservation of the size of the original nuclei implies that the system must have maintained its binary character throughout the reaction phase. The energy lost from the relative motion appears as excitation energy in the two reaction products, which after the reaction dispose of this excitation by various processes, typically neutron evaporation followed by emission of γ rays.

On the one side, damped nuclear reactions are distinguished from the gentler quasi-elastic reactions by their large energy loss, while, on the other side, their binary character distinguishes them from reactions in which a mononucleus is formed, such as fast fission or compound nuclear reactions.

Apart from this distinction, the damped nuclear reactions are also distinguished from the more violent reactions which take place when the bombarding energy is increased. To give the reader an impression of the richness of nuclear reactions, a brief overview of the physical phenomena encountered in damped nuclear reactions as well as in the more violent reactions is given in section 2 of the present paper.

Atomic nuclei exhibit a variety of excitations, and different theoretical descriptions of damped nuclear reactions ascribe the energy loss to the excitation of different types of excitations. In section 3 an overview is given of the most important theories, with special emphasis on nucleon exchange transport.

Nucleon exchange transport has recently been applied to the study of the dynamics of angular momentum during damped nuclear reactions, Døssing 1985a, and it was found that the angular momentum carries characteristic and important information about the reaction process. This development is briefly reviewed in section 4, and section 5 discusses variances in energy loss and scattering angle, which are relevant for differential cross sections. In section 6 theoretical differential cross sections and results for the polarisation of γ rays emitted by the reaction products after the reaction are compared to experiment, thereby widening the confrontation of the theory with data. Section 7 gives a conclusion, and the appendix gives the technical details of the γ ray polarisation calculation and discusses the quality of the information contained in γ ray polarisation observations as compared to the observation of angular distributions of continuum γ rays.

Most of section 2 of the present paper is meant to be accessible for readers without pre-knowledge of nuclear physics. Section 3 is also quite general, but enters into more special topics. The remaining sections as well as the appendix deal with specialized problems. They are centered around the presentation of new results in section 6, and the conclusion drawn from them in section 7.

2. Survey of reactions between heavy ions

Figure 1 illustrates nuclear reactions between heavy nuclei for different bombarding energies, starting with the smallest in the top row and ending with the largest in the bottom row. The left hand column shows the two nuclei approaching each other, and the length of the arrow indicates the velocity in the center of mass frame. The middle column shows schematically the nuclei in a characteristic moment of their interaction. Understanding the physical processes at that moment is the aim of nuclear reaction studies, but in experiments information can only be obtained through careful observation of nuclei, γ rays or other reaction products. The end of the reaction phase is illustrated in the right hand column. The reaction products are still close together, but they move with high speed, about to start their journey out to the detectors, where their type, energy etc. may be determined.

The length scale of the illustration is given by the nuclear radii, which are around 5 to 8 fm (1 fm = 10^{-15} m), and the reaction times are of the order of 10^{-21} to 10^{-23} sec.

For the lowest row, labelled by the name ultrarelativistic collisions, the bombarding energy is so large that the velocities of the nuclei are only slightly smaller than the velocity of light. The nuclei approaching each other in the lower left hand corner are really the same as the ones illustrated in the rows above, but because of their high velocity they are contracted along their direction of motion.

A general reference to reactions between heavy nuclei with emphasis on theoretical questions may be found in the proceedings of a conference held in Paris in May 1984, Martinot 1984.

2.1. Basic properties of stable nuclei

By letting heavy nuclei react with each other, one can study the matter inside nuclei under conditions which are fundamentally different from those present in stable nuclei. Stable nuclei consist of protons and neutrons, or with their common name, *nucleons* (and of virtual particles associated with the mutual interaction of the nucleons). Stable nuclei have an interior of almost constant density of nucleons, and a thin surface region over which the density falls from the value in the interior down to values close to zero. The interior density is practically independent of the size of the nucleus. The thickness of the surface region is approximately 1 fm, which is small compared to the radius of around 6 fm, so for an illustration it is quite realistic to draw the nuclei as having

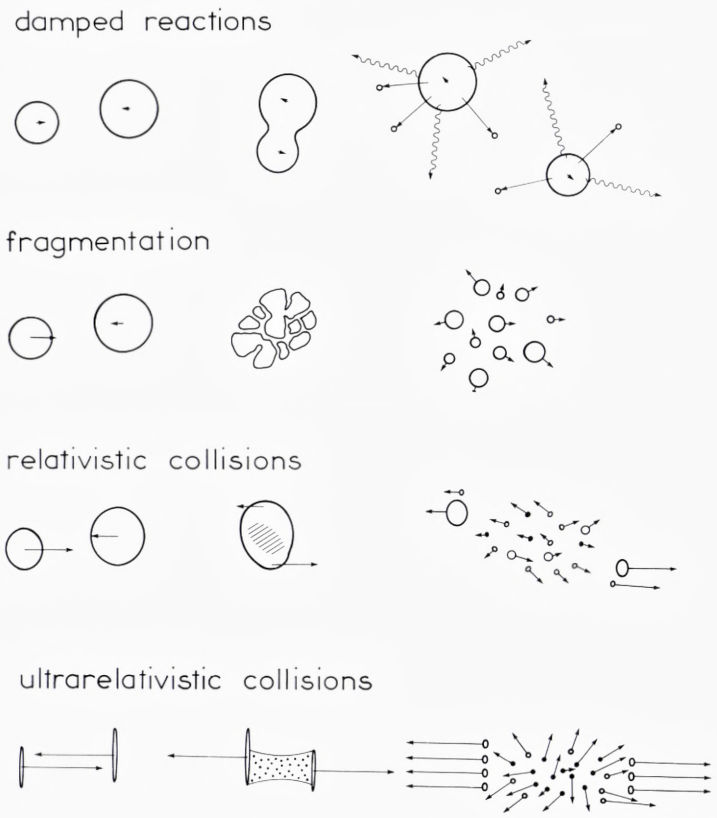

Fig. 1. Schematic illustration of heavy ion reactions. The 4 rows show the time evolution for different sizes of the bombarding energy. The left hand picture shows the nuclei approaching each other, the middle one shows a characteristic moment of the reaction, and finally the right hand picture shows the end of the reaction phase. Open circles or ellipsoids denote nuclei or nucleons, and filled dots denote pions or other particles produced during the reactions.

sharp surfaces. The interaction between nucleons contains both attraction and repulsion, depending on their state of relative motion. The size of stable nuclei balances the attraction and repulsion.

Each nucleon moves in the common attractive potential generated by the interaction with the others. In the simplest picture of nuclei, the lowest nucleon eigenstates in the potential are filled up according to the Pauli principle.

2.2. Energy scales for elastic and inelastic nucleon collisions

The energy unit commonly used in nuclear physics is MeV. (For example the energy released in the fission of one Uranium nucleus is approximately 150 MeV).

Due to the Pauli principle two nucleons in a stable nucleus can not collide and scatter to two new levels. In a reaction between heavy nuclei, all nucleons can move in the common time dependent potential generated by the nucleon distribution. To assess the relative importance of the motion in the potential versus collisions between individual nucleons, the energy per nucleon in the relative motion of the nuclei should be compared to the depth of the potential of approximately 45 MeV, and to the kinetic energy of around 35 MeV of the nucleon occupying the highest level.

For slowly moving nuclei most of the collisions possible for free nucleons will be hindered by the Pauli principle, since there will generally not be energy enough in the relative motion of most pairs of nucleons from the two nuclei to scatter into unoccupied levels. The nucleons will then move with relatively long mean free path between collisions. This applies to the damped reactions where the energy per nucleon is around 4 MeV, and also to some extent to the fragmentation reactions.

For rapidly moving nuclei, the energies of the nucleons are so high that a potential of the order of 45 MeV only will deflect their direction of motion very little, and only few collisions between pairs of nucleons taken from the two different nuclei will be hindered by the Pauli principle. This applies to the relativistic and ultrarelativistic collisions.

Other energy scales are set by the threshold energies for inelastic collisions between nucleons in which other particles are created, or the nucleons themselves are excited or changed. Each nucleon is believed to consist of three smaller particles, quarks. During violent collisions, two quarks can interact and change their nature, and pairs of quarks and antiquarks can be created. For example, a neutron and a proton can collide, forming two protons and a pion, which consists of a quark and an antiquark bound together. The threshold energy for such processes is given by the rest mass energy of the lightest particles which can be created, the pions, 140 MeV.

2.3 Damped reactions

In damped nuclear reactions the nuclei approach each other with a relative energy of the order of 4 MeV per nucleon. During the reaction the nuclear surfaces attract each other and start to overlap, but they do not have energy to penetrate each other because this would lead to a high density and a repulsive potential in the region of overlap. Instead, the density between the two nuclei forms a smooth continuation of their interior densities during most of the reaction. Due to the relative motion

of the nuclei, nucleons can move from an occupied level in one nucleus to an unoccupied one in the other. Quite many nucleons may be exchanged this way, and through collisions with nucleons in the nucleus receiving them, they will heat the nuclei up. Still their energy in the receiving nucleus will not be very high, so most collisions are hindered by the Pauli principle, and the nucleons will have an average mean free path of the order of the nuclear radius before colliding.

The exchange of many nucleons between the two nuclei in motion and the simultaneous heating pose many intriguing problems, which we shall touch upon in the next section. Also other excitations than nucleon exchange will occur, such as substantial deformations of the surfaces of the nuclei. On the other hand, the heat per nucleon produced is small compared to the binding energy of the nucleons in the nuclei, and such quantities as the density inside the nuclei are practically not changed during the reaction.

Some theories of nuclear reactions yield quite definite results for the time evolution of charateristic variables. This is for example shown in section 4 of the present paper, which deals with the application of nucleon exchange transport theory to describe the dynamics of the rotation of the nuclei during the reaction.

2.4. Fragmentation reactions

Increasing the energy to around 75 MeV per nucleon, a large excitation energy may be developed, caused by the more frequent collisions possible between the nucleons. Many collisions will tend to thermalize the velocity distribution over the volume of the reacting nuclei. Above a certain temperature, the nuclear matter will not be stable any longer, and it will expand and crack, leading to a fragmentation of the two colliding nuclei. These cirumstances are reminiscent of the situation in the hot matter in supernovae as it expands again after a strong compression. The important questions are the evaluation of the critical temperature for fragmentation and of the distribution of the sizes of the smaller nuclei produced in the fragmentation.

2.5. Relativistic collisions

Increasing the energy per nucleon still further, up to around 500 MeV per nucleon, the velocities of the nuclei before colliding are of the order of 60% of the speed of light, hence the name relativistic collisions. As we have argued, at these energies the reaction will be dominated by collisions between the nucleons. When the nuclei jam into each other, the

nucleons on the sides of the nuclei facing each other will collide first, acquiring sidewards motion at the expense of their velocity along their original direction of motion. Some of the collisions will be inelastic. The nucleons are then not able to leave the interaction zone as quickly as they entered, while nucleons which have not yet collided are still streaming in from the back sides of the nuclei. This results in a substantial buildup of the density, pictured as the hatched area in the center of the nuclei in the reaction phase shown in fig. 1. The density may reach 4 times the normal density inside nuclei. According to most theories of nucleon interactions and nuclear matter, this will result in a strongly repulsive potential in the region of high density, which for the geometry of the collision depicted in fig. 1 will deflect the nucleons moving in from the left downwards, and upwards for the nucleons moving in from the right. The repulsive potential will also tie up a substantial fraction of the kinetic energy of the nucleons into potential energy. Collisions between these nucleons will then be less energetic and result in the production of fewer pions than would be produced if the repulsion was not there.

Towards the end of the reaction, parts of the original nuclei have not suffered collisions, and they move on as smaller heated nuclei. The nucleons which have collided form a gas of nucleons, reminiscent of the situation in the early universe. The gas will expand, and some nucleons may combine to form light nuclei, like ^{2}H, ^{4}He etc. The velocity distribution will still carry memory of the deflection by the repulsion caused by the high density, and the pions will be fewer also beause of this repulsion.

Both the number of pions and the velocity distributions have recently been observed and related to the repulsion associated with the hot dense nuclear matter.

2.6. Ultrarelativistic collisions

Increasing the energy of relative motion considerably further, up to around 20000 MeV per nucleon, the reaction is believed to change its nature completely. At these energies the nuclei are contracted to flat discs. As the two discs pass each other the more violent of the nucleon collisions may first produce an interaction quantum, a gluon string, between the quarks which have interacted. The other two quarks in each of the nucleons do not feel the interaction immediately. The gluon strings later break up, producing showers of particles, and the space between the flat discs will be filled with a highly energetic mixture of quarks and antiquarks and gluons. If the density and temperature in this

region becomes high enough, the quarks and antiquarks will no longer be confined to each other within particles like pions or nucleons, but they will be able to move freely within a »superbag« whose boundaries are indicated in the middle part of the last row of fig. 1.

Having many quarks and antiquarks together in a hot medium within the superbag may be one of the best ways one can learn about these fundamental building blocks of matter and their interaction.

The situation at the boundary of the superbag poses many questions, how will the hot plasma inside the superbag cool off and return to ordinary matter where the quarks are confined within little bags in nucleons or pions etc. No matter how it happens, an enormous shower of particles will be produced in the final phase of the reaction. Until now reactions with these high energies have only been recorded in very few cases on photografic plates where nuclei from cosmic rays have hit nuclei in the emulsion on the plates. Accelerators for the study of these reactions are only proposed at the moment, and it is still not known whether the conditions for producing the superbag will be achieved. Also it is being debated which observation among the many particles formed will give the best diagnostics whether a superbag was formed. The conditions within the superbag and during the return to the final reaction products are reminiscent of the conditions in the very early universe.

3. Theories of damped nuclear reactions

As was argued in section 2, collisions between nucleons are suppressed in damped nuclear reactions, and the dynamics will be dominated by the motion of nucleons in the time dependent mean field.

3.1. Time dependent Hartree-Fock

The time dependent Hartree-Fock theory provides an extreme description of damped nuclear reactions in terms of independent particle motion in the average potential. The wave function for the whole colliding system is at all times a Slater determinant, and the time evolution of the independent particle wave functions occupied by nucleons is given by the Schrödinger equation. Thus collisions between nucleons, leading to more complicated states, are not possible, entropy is not produced, and heating of the nuclei will not take place in the strict sense.

Nevertheless, in applications to damped nuclear reactions, time dependent Hartree-Fock generally gives a good account of the energy loss,

and of the relation between energy loss and average scattering angle. Intuitively, one can say that the energy loss comes about because of the inelastic collisions of the nucleons with the time dependent potential. This time dependence is displayed in pictures. Davies 1981, of the evolution of the calculated density distribution.

More detailed investigations, Köhler 1979, Tang 1981, of the damping mechanism in time dependent Hartree-Fock have applied the Wigner transformation, which transforms the one body density matrix into a phase space distribution. From these investigations it is apparent that transfer of nucleons between the two nuclei play a crucial role for the damping. Since the two nuclei move relative to each other, the momentum distribution of nucleons in the two nuclei are shifted relative to each other, as illustrated in the right hand side of figure 2. This allows phase space points to move from one nucleus to unoccupied parts of the phase space in the other. Also, the boundaries of the potential may move relative to the momentum distribution of phase space points which are close to the boundary, and in this case phase space points may be reflected from the boundary into previously unoccupied points of the phase space distribution.

Both of these kinds of inelastic interactions of nucleons with the time dependent potential give rise to damping. They were first discussed by Swiatecki and coworkers, Blocki 1978, and named *window friction* and *wall friction,* respectively. This was not by using time dependent Hartree-Fock, but by more schematic and general arguments.

Attempts to explain the mass dispersion observed in damped nuclear reactions with the Slater determinant wave function of the system after the reaction phase failed, Davies 1978. This is understood not to be a failure of the mean field description, but specifically due to the restriction to this type of wave function, Dasso 1979. Generally dispersions cannot be addressed by time dependent Hartree-Fock as applied so far, but recent theoretical developments may improve this situation, Balian 1984.

The density distribution calculated with time dependent Hartree-Fock displays quite substantial deformations of the nuclear surfaces, especially when the nuclei are about to separate at the end of the reaction phase. This enables the nuclei to separate with kinetic energies appreciably below the Coloumb barrier for spherical nuclei, in accordance with experiment. Surface vibrations of the nuclear shape are automatically present in time dependent Hartree-Fock calculations.

3.2. Transport theories

Realistic time dependent Hartree-Fock calculations for damped nuclear reactions were long in the making, and were preceded by theories which treated the time dependent field more schematically, but which, on the other hand, also addressed heating of the nuclei. The first such theory was derived by Nörenberg and coworkers, Nörenberg 1975, Ayik 1976. In this work the characteristic time for quantal phase correlations to die out was found to be considerably shorter than the time scale for changes of a set of macroscopic variables. Generally, phase correlations may survive for a while, but those influencing the time evolution of the macroscopic variables are short. This enables the use of a master equation, or transport equation, for the distribution of macroscopic variables, and further, a Fokker-Planck equation for the mean values and covariances of the macroscopic variables. A recent review of these developments with references to the earlier work is contained in reference Nörenberg 1982, which also treats a novel revision of the theory for rather gentle collisions, based upon considerations of the time for specific correlations to die out. A review of the various early formulations of irreversibility and transport theories for damped nuclear reactions has been given by Weidenmüller 1980.

In these theories, the basic excitations giving rise to transport are, in accordance with the overall independent particle picture, taken as inelastic particle-hole excitations within nuclei and nucleon transfers between them. To obtain closed expressions for coefficients, and for the phase correlations to die out fast, the interaction matrix elements for these excitations were taken as Gaussian distributed and with random signs. Microscopic calculations justified this to some extent, Barrett 1978, Shlomo 1979.

Transport theories have been very successful in explaining the width of the mass distribution, Ayik 1976, Wolschin 1981, and later some features of the spin distribution, Wolschin 1978, Wolschin 1981. Also differential cross sections could be reproduced quite well, Agassi 1978, Ko 1979.

3.3. Coherent surface excitation description

A somewhat different description of damped nuclear reactions treats the inelastic particle-hole excitations within the nuclei in a more specific way. When subject to an external field, like the Coulomb and nuclear field from the other nucleus, the particle-hole states will not be excited in a random way, but rather in certain superpositions, collective vibration

states. Within the Coherent surface excitation model, Broglia 1981, specific account is taken of collective surface vibrations. These vibrations correspond to standing waves on the nuclear surface. In actual applications of the coherent surface excitation theory, a low energy and a high energy vibration for each multipolarity from 2 up to around 5 are included. The mean excitation energy and rate of damping of each vibration are taken in accordance with both theoretical estimates and experimental systematics.

It is a big advantage of this description that the deformation of the surfaces are included, being determined by the amplitudes for the vibrations. As in time dependent Hartree-Fock calculations, substantial distortions of the density distribution at the end of the reaction phase lead to final energies below the Coulomb barrier for the exit phase of the reaction, in accordance with experiment. Quantal fluctuations associated with the excitation of the surface modes are found to yield considerable dispersions in quantities such as the energy loss for given impact parameter, Esbensen 1977. This is supported by experiments.

3.4. Nucleon exchange transport

An essentially parameter-free description of nucleon transfers in damped nuclear reactions is given by the nucleon exchange transport theory, Randrup 1979, Randrup 1982.

The theory is based upon transport theory, and in the formal derivation of transport coefficients for one-body operators, the time development of the system is followed during a small time interval. The nucleon transfers are described to take place between eigenstates of the mean fields of the individual nuclei by means of the interaction one body field, which is localized in the region of spatial overlap between the nuclei. A transferred nucleon will occupy an excited state in the new nucleus and leave a hole state behind in the old, and both of these will be damped by collisions with nucleons and with the moving potential boundaries. This damping is assumed to be so fast that the density operator is kept on diagonal form in the eigenstates of the mean fields of the nuclei, given by thermal excitation. This and other approximations applied in the derivation will be valid in the limit of slow reactions between very large nuclei. Especially important is the replacement of matrix elements of the interaction potential by a classical flow of phase space points.

The approximations have clear physical content, but some of them are difficult to justify in a strict sense. Most serious seems to be the argumentation that energy is conserved in the transfers, when referred to a

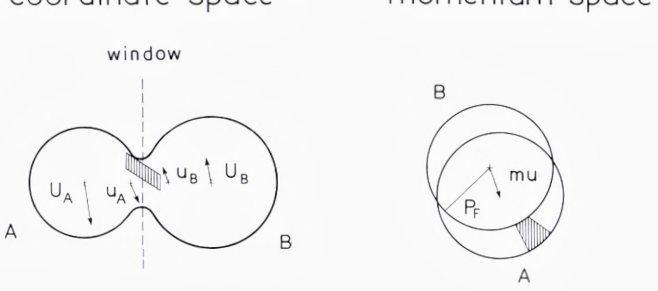

Fig. 2 Illustration of transfer of a phase space interval between two nuclei. See the text for details.

common reference frame. For example, this requires the transferring potential to act undisturbed within a time interval of the order $\Delta t \approx 1.6\times10^{-22}$ sec to achieve energy conservation to the accuracy of 2 MeV. This time interval is only slightly smaller than typical time scales for substantial changes in mean values and variances of for example the spin variables of the nuclei.

The transfer of phase space points is illustrated in figure 2, in which the left hand part shows the geometry of the dinuclear system at a certain moment in a reaction. The centers of the nuclei A and B move with velocities $\vec{U}_A$ and $\vec{U}_B$, respectively. Due to the slowing down of the orbital angular momentum during the reaction, the local velocities in the nuclei at the window, $\vec{u}_A$ and $\vec{u}_B$, may be smaller. The hatched area symbolizes the coordinate part of a phase space interval situated around the window plane, which has the possibility of being transferred from B to A or the other way. The right hand part of the figure illustrates the momentum space. The phase space points are filled up according to the Pauli principle, within spheres in momentum space for given coordinate points. The relative motion displaces the spheres relative to each other by the amount $m\vec{u} = m(\vec{u}_A - \vec{u}_B)$, m being the nucleon mass. The hatched area symbolizes the momentum part of the phase space interval, being occupied in nucleus A and not in B. With increasing excitation, the Fermi spheres acquire a diffuse surface, the diffuseness being determined by the temperature τ in the nuclei. Even for the case of no relative motion, nucleon exchanges are then still possible between occupied and unoccupied parts of the phase space in the nuclei, the number of such exchanges being proportional to the temperature. For the general case with both a relative velocity and a temperature, the number of exchanges is given by the *effective temperature* $\tau^\star$, defined as

$$\tau^\star = \left\langle \tfrac{1}{2} |\vec{u} \cdot \overleftarrow{p}| \coth\left(\frac{|\vec{u} \cdot \overleftarrow{p}|}{2\tau}\right) \right\rangle_F \qquad (3.1)$$

where F symbolizes an average over the Fermi sphere of the nuclei and over the window area. In expression (3.1) as well as in the drawing of fig. 2 we have for simplicity neglected differences in the Fermi momenta of the two nuclei.

The transport coefficients contain two types of variables: (i) basic nuclear paramenters, such as the Fermi momentum. (ii) dynamic variables, such as the effective window area, the distance between the centers of the nuclei, the radial momentum of the relative motion etc.

The theory has been successfully applied for studying the mass and charge distributions, Schröder 1981, Britt 1982, and good accordance was also generally found with experiments on the spin distribution, Døssing 1985b. The present application to Wilszinsky plots and γ ray polarisations presents a continuation of these comparisons of the theory with data.

3.5. Statistical models

No matter which excitations are primarily responsible for the main part of the energy loss in damped nuclear reactions, their clean characteristics get lost and cannot be observed because of the thermalisation within the nuclei. For example, in the hot nuclei leaving the reaction, an excited surface vibration will not decay by emission of a γ ray of a specific energy. It will instead get dissolved by coupling to the complicated excitations present in the hot nucleus.

Therefore, in addition to the variables describing the relative motion of the nuclei after the reaction, only variables which are conserved in each nucleus after the reaction due to general principles can be studied experimentally. These are the mass and charge, the angular momentum, (and the parity, which is of little use).

If the reaction time is long enough, the distribution in some of these variables will just be given by statistical excitation, governed by the temperature in the dinuclear system. In this case no information on the primary excitation mechanism survives. Fortunately, it is clear for the mean values of both neutron number, proton number and spins that statistical excitation is not generally achieved. It is only for the second moments of the spin distribution that a statistical model has been formulated and applied for all kinetic energy losses, Moretto 1980, Schmidt 1982. For large energy losses, statistical excitation of the mean spins has also been proposed, Moretto 1984.

The statistical model for the mean spin vector explains well the spin sizes as function of the mass partition in a number af reactions, and also

the model for the variances yields good agreement with quite many experiments, Moretto 1984. However, in our recent analysis, Døssing 1985a,b, the statistical model for the spin distribution is found to predict that the direction of the major in-plane spin variance is a specific function of the scattering angle. The characteristic differences in relaxation times for the various spin modes implied by our dynamical equations, which we shall discuss in the next section, yield a different, but also specific result for this direction. Experiments on the in-plane sequential fission fragment angular distributions, which determine this direction, agree with the dynamical results and disagree with the statistical model.

4. Nucleon exchange transport for spin variables

When applying the Fokker-Planck equation to angular momentum variables, the choice of coordinate system is important. The coordinate system applied here follows the geometry of the dinuclear system, i. e. it is a *body-fixed coordinate system*. The z-axis is along the radius vector of relative motion, and the y-axis is along the orbital angular momentum. Seen by an external observer, this coordinate system turns because of the the orbital rotation and fluctuates because the direction of the orbital rotation may change during the reaction.

General expressions for the transport coefficients of one body operators are given in Randrup 1979, and coefficients for angular momentum transport are presented in Randrup 1982. Finally, the derivation of the transport equations with respect to this coordinate system as well as expressions for transforming the spin moments to the laboratory system are given in Døssing 1985a.

We shall not here repeat the formal development, but rather define the variables and discuss the transport coefficients entering the equations. This will be followed by a discussion of the appearence of the equations and the characteristics of their solutions in terms of relaxation times for the spin variables.

4.1. Spin variables and mobility tensors

We consider the time evolution of the distribution of spins in the two nuclei, $\vec{S}^A$ and $\vec{S}^B$, and the orbital angular momentum $\vec{L}$. With the coordinate system applied, $\vec{L}$ has no x and z components. From the symmetry of the problem, mean values along the x and z axis must be

zero, and also covariances between y components and other components must vanish. Thus, restricting to the first and second moments, the following can be different from zero:

$$\begin{aligned} &\langle S_y^A\rangle,\ \langle S_y^B\rangle,\ \langle L_y\rangle \\ &\sigma_{yy}^{FG}\ ,\ F,G = A,B,L \\ &\sigma_{xx}^{FG}\ ,\ \sigma_{xz}^{FG}\ ,\ \sigma_{zz}^{FG}\ ,\quad F,G = A,B \end{aligned} \tag{4.1}$$

where, for example, $\sigma_{yy}^{AL} \equiv \langle (S_y^A - \langle S_y^A\rangle)(L_y - \langle L_y\rangle)\rangle$.

As in reference Randrup 1982, a compact notation is achieved by defining the transport coefficients in terms of mobility tensors:

$$\begin{aligned} \overleftrightarrow{M}^{AA} &= mN(a^2\overleftrightarrow{T} + c_{ave}^2\overleftrightarrow{I}) \\ \overleftrightarrow{M}^{AB} &= mN(ab\overleftrightarrow{T} - c_{ave}^2\overleftrightarrow{I}) = \overleftrightarrow{M}^{BA} \\ \overleftrightarrow{M}^{BB} &= mN(b^2\overleftrightarrow{T} + c_{ave}^2\overleftrightarrow{I}) \end{aligned} \tag{4.2}$$

Here m is the nucleon mass and N is the total flow of nucleons across the window, being proportional to the total flux inside nuclei times the effective window area. The distances from the centers of the nuclei to the window plane are given by a and b respectively, the sum a+b being equal to the dinuclear separation R. c_{ave} is the average off-axis displacement on the window. $\overleftrightarrow{I}$ is the identity tensor, in terms of unit vectors along the coordinate axises $\overleftrightarrow{I} \equiv \hat{x}\hat{x}+\hat{y}\hat{y}+\hat{z}\hat{z}$, and $\overleftrightarrow{T} \equiv \hat{x}\hat{x}+\hat{y}\hat{y}$ projects on the plane perpendicular to the dinuclear axis. Starting with zero variances $\sigma_{ij}^{FG}(t=0)=0$, the time evolution of the spin variances during the first small time interval Δt is given by

$$\overleftrightarrow{\sigma}^{FG}(\Delta t) = 2\tau^\star\overleftrightarrow{M}^{FG}\,\Delta t \tag{4.3}$$

where $\tau^\star$ is the effective temperature (3.1). It is natural that the increase in variances are proportional to $\tau^\star$, which measures the part of the momentum space available for transfers. The mobility tensors describe how easily the nucleon exchange can build up spin along the various directions in the two nuclei. The transverse directions are clearly preferred for the direction along the dinuclear axis. Figure 2 may illustrate this. Considering the various directions of the momentum and locations on the window, values of $\vec{r}\times\vec{p}$ relative to the center of nucleus A for the nucleons being able to transfer are seen to be generally larger along the transverse directions than along the dinuclear axis.

Since the total angular momentum $\vec{J} = \vec{L}+\vec{S}^A+\vec{S}^B$ has to be conserved, equation (4.2) implies the following expressions for mobility tensors involving the orbital angular momentum $\vec{L}$:

$$\begin{aligned}
\overleftrightarrow{M}^{AL} &= -\overleftrightarrow{M}^{AA} - \overleftrightarrow{M}^{AB} = -\,mNaR\overleftrightarrow{T} = \overleftrightarrow{M}^{LA} \\
\overleftrightarrow{M}^{BL} &= -\overleftrightarrow{M}^{AB} - \overleftrightarrow{M}^{BB} = -\,mNbR\overleftrightarrow{T} = \overleftrightarrow{M}^{LB} \\
\overleftrightarrow{M}^{LL} &= -\overleftrightarrow{M}^{LA} - \overleftrightarrow{M}^{LB} = mNR^2\overleftrightarrow{T}
\end{aligned} \tag{4.4}$$

It is convenient to discuss together with the standard spin variables $\vec{S}^A$, $\vec{S}^B$ also the absolute and relative spins in the nuclei $\vec{S}^+$ and $\vec{S}^-$:

$$\begin{aligned}
&\vec{S}^+ = \vec{S}^A + \vec{S}^B\ ,\ I_+ = I_A + I_B \\
&\vec{S}^- = I_- \left(\frac{\vec{S}_A}{I_A} - \frac{\vec{S}^B}{I_B} \right),\quad I_- = \frac{I_A I_B}{I_A + I_B}
\end{aligned} \tag{4.5}$$

where I_A, I_B, I_+, and I_- denote moments of inertia, For I_A and I_B we apply rigid body moments of inertia, which are the relevant ones for heated nuclei. The kinds of rotational motion of the dinuclear system measured by the spins $\vec{S}^+$ and $\vec{S}^-$ have been given illustrative names. The *wriggling modes* describe rotations of the two nuclei in the same sense perpendicular to the dinuclear axis, which gives non-zero values of S_x^+ or S_y^+. Non-zero values of S_z^+ measure the motion of the *tilting mode,* and S_x^-, S_y^- measure the motion of the *bending modes*, and S_z^- the *twisting mode.* These names were given by Nix and Swiatecki, Nix 1965, in a study of nuclear fission, except for the tilting mode, named by Moretto, Moretto 1980, in the formulation of the statistical model for damped nuclear reactions. The mobility tensors in these variables are easily derived from those in the standard variables

$$\begin{aligned}
\overleftrightarrow{M}^{++} &= \overleftrightarrow{M}^{LL} = mNR^2\overleftrightarrow{T} = -\overleftrightarrow{M}^{+L} \\
\overleftrightarrow{M}^{+-} &= mNR\left(\frac{I_A b - I_B a}{I_A + I_B} \right) \overleftrightarrow{T} = -\overleftrightarrow{M}^{-L} \\
\overleftrightarrow{M}^{--} &= mN\left(\frac{I_A b - I_B a}{I_A + I_B} \right)^2 \overleftrightarrow{T} + mN\, c_{ave}^2 \overleftrightarrow{I}
\end{aligned} \tag{4.6}$$

Since $\overleftrightarrow{M}^{++}$ only has components along the transversal directions, the tilting mode does not receive excitation directly by nucleon transfer. For symmetric reactions, a=b and I_A=I_B, the mobility tensor $\overleftrightarrow{M}^{+-}$ vanishes, and the time evolution in $\vec{S}^+$ and $\vec{S}^-$ will be decoupled.

4.2. Equations of motion

The following transport equations for the spin distributions are derived in Døssing 1985a:

$$\dot{S}_y^F = -\sum_G (M_t^{FG} S_y^G + \frac{1}{L_y}\sigma_{xx}^{FG} M_t^{GL})/I_G + \frac{\tau^\star}{L_y}(2M_t^{FL} - \frac{S_y^F}{L_y} M_t^{LL})$$

$$\dot{\sigma}_{xx}^{FH} = 2\tau^\star M_t^{FH} - \sum_G (\sigma_{xx}^{FG} M_t^{GH} + M_t^{FG} \sigma_{xx}^{GH})/I_G - \omega_R(\sigma_{xz}^{FH} + \sigma_{zx}^{FH})$$
$$- \frac{S_y^F}{L_y}(2\tau^\star M_t^{LH} - \sum_G M_t^{LG} \sigma_{xx}^{GH}/I_G) - (2\tau^\star M_t^{FL} - \sum_G \sigma_{xx}^{FG} M_t^{GL}/I_G)\frac{S_y^H}{L_y}$$
$$+ 2\tau^\star \frac{S_y^F}{L_y} M_t^{LL} \frac{S_y^H}{L_y}$$

$$\dot{\sigma}_{yy}^{FH} = 2\tau^\star M_t^{FH} - \sum_G (\sigma_{yy}^{FG} M_t^{GH} + M_t^{FG} \sigma_{yy}^{GH})/I_G \qquad (4.7)$$

$$\dot{\sigma}_{zz}^{FH} = 2\tau^\star M_n^{FH} - \sum_G (\sigma_{zz}^{FG} M_n^{GH} + M_n^{FG} \sigma_{zz}^{GH})/I_G + \omega_R(\sigma_{xz}^{FH} + \sigma_{zx}^{FH})$$

$$\dot{\sigma}_{xz}^{FH} = -\sum_G (\sigma_{xz}^{FG} M_n^{GH} + M_t^{FG} \sigma_{xz}^{GH})/I_G - \omega_R(\sigma_{xx}^{FH} - \sigma_{zz}^{FH})$$
$$+ \frac{S_y^F}{L_y}\sum_G M_t^{LG}\sigma_{xz}^{GH}/I_G$$

Here the brackets around mean values have been omitted for notational simplicity, ω_R denotes the angular velocity of the orbital rotation. $\omega_R = \frac{L_y}{I_R}$ and M_t^{FG} and M_n^{FG} denote mobility tensors along the transversal and the normal direction, respectively. The sums over the index G run over G = A,B,L, or over G = +, –, L. All terms containing ω_R or $\frac{1}{L_y}$ as factors are due to the special choise af the body fixed coordinate system. The orbital rotation perpendicular to the y axis causes a redefinition of the x and z axises, being taken into account by the terms containing ω_R. The terms containing L_y in the denominator arise from the fluctuation in the direction of $\vec{L}$ caused by the nucleon exchange, and they are derived under the assumption that L_y^2 is large compared to all variances.

4.3. Stationary solution and relaxation times

For given total angular momentum J one can prove that the equations (4.7) have a unique stationary solution given by

$$\langle L_y \rangle = \frac{I_R}{I_0} J \;, \qquad \overleftrightarrow{\sigma}^{LL} = \tau^\star I_+ \frac{I_R}{I_0} \hat{y}\,\hat{y} \qquad (4.8)$$

$$\langle S_y^+ \rangle = \frac{I_+}{I_0} J - \tau^\star I_+ \frac{I_0}{I_R}\frac{1}{J}, \qquad \overleftrightarrow{\sigma}^{++} = \tau^\star I_+ \frac{I_0}{I_R}(\hat{x}\hat{x} + \hat{z}\hat{z}) + \tau^\star I_+ \frac{I_R}{I_0}\hat{y}\hat{y}$$

$$\langle S_y^- \rangle = 0 \;, \qquad \overleftrightarrow{\sigma}^{--} = \tau^\star I_- \overleftrightarrow{I}$$

In these expressions $I_0 = I_R + I_A + I_B$ is the total moment of inertia of the dinuclear system. During the reaction the moments of the spin distribu-

tion will at each instant evolve towards these equilibrium values, which in turn vary in time due to the time dependence of the effective temperature $\tau^\star$ and of the moment of inertia for the orbital rotation I_R.

The mean values of the stationary solution correspond to a rigid rotation of the dinuclear complex.

The solutions (4.8) for the variances correspond to statistical excitation of the spin modes, however with the temperature associated with the heat, τ, replaced by the effective temperature $\tau^\star$.

Typical time scales, *relaxation times,* for the approach to the stationary values can be obtained by dividing the stationary solution (4.8) by the corresponding initial time derivative, as for example given in equation (4.3) for the variances.

For a symmetric collision for which the motion in $\vec{S}^+$ and $\vec{S}^-$ are decoupled, this gives the following relaxation time for the wriggling modes

$$t_{++} = \frac{\tau^\star I_+}{2\tau^\star M_t^{LL}} = \frac{I_+}{2mNR^2} \tag{4.9}$$

and for the three negative modes

$$t_{--} = \frac{\tau^\star I_-}{2\tau^\star M^{--}} = \frac{I_-}{2mNc_{ave}^2} \tag{4.10}$$

The time evolution of the tilting mode is more complicated, since σ_{zz}^{++} only receives contributions indirectly from σ_{xx}^{++} through the orbital rotation. The relaxation time for the tilting mode is then determined by finding the eigenvalues of the linear system of equations for σ_{xx}^{++}, σ_{xz}^{++} and σ_{zz}^{++}, and the main part of $\sigma_{zz}^{++}$is found to approach equilibrium with the relaxation time

$$t_{+z} \simeq \left(4\omega_R^2 \frac{L_y}{J} t_{++}\right)^{-1} \tag{4.11}$$

The relaxation time for the mean values $\langle S_y^+ \rangle$ and $\langle L_y \rangle$ are given by $2t_{++}$

This relation to the statistical model together with the expressions for the relaxation times we consider to be important results of the study in Døssing 1985a, because these results contain some definite predictions of the theory, which can be confronted with data without having to perform detailed calculations.

Inserting typical values of the coefficients appearing in the expressions for the relaxation times, one finds that except for the most peripheral collisions the wriggling modes are expected to reach equilibrium. The relaxation time for the negative modes is substantially longer, and only

for quite central collisions will they come close to equilibrium. The tilting mode receives the strongest excitation for peripheral collisions, due to the occurence of ω_R in the denominator. For more central collisions the tilting mode receives only little excitation. Examples of these relaxation times are shown in Døssing 1985a.

Since the relaxation time for S_y^+ is also quite small and the asymptotic value for this spin is large compared to the equilibrium values of the dispersions, the spin distribution will be dominated by the mean spin for most values of the total angular momentum. For example the average length of the spin vector will for most cases be given by the size of the mean spin vector plus a relatively small correction containing the dispersions.

5. Mean trajectory implementation of nucleon exchange transport

To obtain results for comparing with data, the transport equations (4.7) for the spin distribution are solved together with equivalent equations for the separation R between the two nuclei, the conjugate momentum P and the scattering angle θ. This is done for a grid of values of the total angular momentum J, and subsequently an integration is performed over J to obtain cross sections and spin distributions gated by energy loss and scattering angle.

The degree of contact between the two nuclei during the reaction is related to the geometrical neck connecting them. The neck motion implies a wall friction, and the time evolution of the neck is followed with insertion of the mean values for P and R. Thus, the dynamics with restriction to the mean trajectory determines both the rate of nucleon exchange and thereby the window friction, as well as the wall friction.

Expressions for the Coulomb and nuclear potentials applied can be found in Randrup 1982, and Fokker-Planck equations for the variances are given in Døssing 1985a.

The variances in the variables considered give rise to a variance in the final energy of the relative motion, which must be evaluated at the end of the reaction phase.

After the reaction phase, the two nuclei recede on a Coloumb trajectory, and the average scattering angle can be determined. This angle is inserted into the equations transforming the spin variables from the fixed coordinate system to the external coordinate system. The variance in

scattering angle receives contributions both during the reaction phase and on the Coulomb trajectory, caused by the variances in the orbital angular velocity and in the other dynamical variables determining the angle turned on the trajectory.

For each J, this procedure permits the determination of mean values and covariances for the variables which are of interest experimentally, namely the total kinetic energy loss, the scattering angle, the neutron and proton numbers in one of the nuclei, and the spins in the two nuclei. Denoting these variables by the symbol $\vec{C} \equiv E,\theta,N_A,N_B,Z_A,Z_B,$ $S_X^A,S_Y^A,S_Z^A,S_X^B,S_Y^B,S_Z^B$, we assume that the distribution is Gaussian, (in accordance with the approximations applied to obtain the Fokker-Planck equations):

$$f_J(\vec{C}) = \pi\lambda^2 \frac{2J+1}{(2\pi|\overleftrightarrow{\sigma}|)^6} \exp[-\tfrac{1}{2}(\vec{C} - \langle\vec{C}\rangle)\cdot\overleftrightarrow{\sigma}^{-1}\cdot(\vec{C} - \langle\vec{C}\rangle)] \qquad (5.1)$$

where $\overleftrightarrow{\sigma}$ is the covariance matrix in the variables considered. (Capital letters are used for the axises of the external coordinate system to distinguish from the body fixed system).

In experiments the total angular momentum cannot be determined, so one has to integrate the distribution (5.1) over J, keeping the energy and eventually also the scattering angle fixed, to obtain cross sections and spin distributions gated by E and θ. The technical details of this is given in Døssing 1985a.

5.1. Time evolution of variances in energy loss and scattering angle

For discussing the Wilszinsky plots and γ ray polarisations presented in the next section, it is important to note that the mean trajectory implementation of the theory implies specific results for the variances in energy loss and scattering angle.

The energy of relative motion is given by

$$E = \frac{P^2}{2\mu} + \frac{L^2}{2\mu R^2} + e^2\frac{Z_A\,Z_B}{R} \qquad (5.2)$$

The variance in E is determined by the variances and covariances of the variables entering this expression. Keeping the main terms to first order in $\tau^\star$, and neglecting the usually small terms due to the variation in neutron and proton numbers, one obtains:

$$\sigma_{EE} = E_R'^2\sigma_{RR} + E_P'^2\sigma_{PP} + 2E_R'E_P'\sigma_{RP} + E_{Ly}'^2\sigma_{yy}^{LL} \qquad (5.3)$$

where E_R' denotes the derivative of E with respect to R, taken at the mean trajectory, and likewise for the other derivatives. Inserting the stationary solution (4.8) for σ_{yy}^{LL} and the equivalent stationary solutions from the Fokker-Planck equations for the evolution in R and P, one obtains for the stationary variance in E

$$\sigma_{EE} = \tau^{\star}\left(\tfrac{1}{2}\frac{(V_C + 2T_{tan})^2}{V_C + 3\,T_{tan}} + 2\,T_{rad} + 2\frac{I_+}{I_0}T_{tan}\right) \tag{5.4}$$

$$\approx \tau^{\star}\left(\tfrac{1}{2}V_C + 2\,T_{rad} + \left(\tfrac{1}{2} + \frac{2\,I_+}{I_0}\right)T_{tan}\right) \approx \tfrac{1}{2}\tau^{\star}\langle E\rangle$$

where the three terms in equation (5.2) have been denoted by T_{rad}, T_{tan} and V_C. In the last expression we have used that the Coulomb energy V_C, is appreciably larger than the other contributions to the energy at the end of the reaction phase.

Actually, it takes quite some time for σ_{RR} to relax, so σ_{EE} will usually be smaller than the saturation value (5.4).

Since the scattering angle is a cyclic variable, the equation for the variance in scattering angle has no restoring term. The variance being accumulated during the reaction is determined by the angular momentum evolution according to the equations

$$\dot{\sigma}_{\theta\theta} = 2\frac{\sigma_{\theta L}}{I_R} \tag{5.5}$$

$$\dot{\sigma}_{\theta F} = \frac{\sigma_{yy}^{LF}}{I_R} - \sum_G \frac{\sigma_{\theta G}}{I_G} M_t^{GF}$$

which are derived in Døssing 1985a. These relations imply that $\sigma_{\theta L}$ relaxes within a time scale given approximately by $2t_{++}$, i. e. quite fast, the saturation value being given by

$$\sigma_{\theta L} = \tau^{\star} I_R\left(\frac{I_+}{I_0}\right)^2 M_t^{LL\,-1} \tag{5.6}$$

Thus, after a time of the order of t_{++}, $\sigma_{\theta\theta}$ will grow constantly with the reaction time t:

$$\sigma_{\theta\theta} \approx 2\tau^{\star}\left(\frac{I_+}{I_0}\right)^2 M_t^{LL\,-1}\,t \approx 2t\tau^{\star}\frac{I_+\,I_R}{I_0\,I_0}\cdot\frac{t_{++}}{I_R} \tag{5.7}$$

$$\approx 8\times10^{-5}\,\tau^{\star}tt_{++}\ \text{radians}^2 \approx 0.25\tau^{\star}tt_{++}\ \text{deg}^{\,2}$$

where the units MeV and 10^{-22} sec are applied for $\tau^{\star}$ and the times t and t_{++}, respectively. To obtain the numerical value, a reduced mass of 50

mass units has been used together with the values 2/7 and 5/7 for the ratios between moments of inertia, and the value 10 fm for the center separation R entering I_R.

The variance accumulated along the outgoing Coulomb trajectory is typically of the same size as the variance estimated so far, so roughly we obtain the following estimate of the total variance of the scattering angle

$$\sigma_{\theta\theta} \approx 0.5\tau^{\star}tt_{++} \text{ deg}^2 \tag{5.8}$$

The value of $\tau^{\star}$ to be inserted here should be the average value during the reaction phase.

Both of the above values for the rate of nucleon exchange and the center separation refer to the reaction of $^{86}Kr + {}^{139}La$, and generally the coefficient in (5.8) will scale with the mass of the dinuclear system to approximately the $-5/3$'th power. The relaxation time t_{++} is of the order of 2×10^{-22} sec. and scales with the mass roughly to the 1/3'rd power.

The expression (5.4) for the stationary variance in energy loss is a statistical limit, obtained by inserting the thermal values for the variances in the basic variables, except for the occurence of the effective temperature $\tau^{\star}$ in stead of the heat temperature τ. Apart from this distinction, the result (5.4) will have a general validity for all theories which predict relaxation towards the statistical equilibrium values.

Conversely, the approximate result (5.8) for the accumulated variance in scattering angle is specifically related to the dynamics of the spin evolution, since the relaxation time t_{++} enters.

Feldmeier and Spangenberger, Feldmeier 1984, apply Cartesian coordinates for the relative motion of the two nuclei, but otherwise also the mean trajetory method. Their variances are several times larger than both of the estimates (5.4) and (5.8) for the variances in energy loss and scattering angle, respectively. These estimates provide fair approximations to our calculated variances (to within a factor of 2 for most cases). We do not know what causes this discrepancy between the two different applications of essentially the same theory, but important points may be (i) the slightly different definitions of the effective temperature within the two schemes of calculation, (ii) the apparent lack of relaxation in σ_{yy}^{LL} displayed in figure 6 in Feldmeier 1984.

6. Wilszinsky plots and γ ray polarisations

6.1. Wilszinsky plots

Figure 3 shows contour plots (Wilszinsky plots) of the differential cross section as function of scattering angle and energy loss, together with the experimental result, Vandenbosch 1978, for the reaction 710 MeV ^{86}Kr + ^{139}La. Also, the mean scattering angle and energy loss is shown for every 20 units of total angular momentum on the calculated plots. Plots (b) and (c) are obtained with two different prescriptions for the reduction of the wall friction caused by the motion of the neck connecting the two nuclei. Plot (b) is obtained with the standard reduction in the neck damping, Randrup 1982, which is effective for long thin necks, and in the calculation for plot (c), full neck damping is applied. Below a total angular momentum close to 100 units, the reactions lead to capture according to the calculation.

6.2. Comparison of calculated and experimental Wilszinsky plots

The experimental Wilszinsky plot clearly displays two components of the cross section, one at small and one at large energy losses.

The contours for the small energy loss component form a long hill stretching from a scattering angle around 35° at energy loss 0 down towards angle 0° at an energy loss of approximately 250 MeV. In the calculated results, the ridge of the hill is defined by the curve running through the points of mean scattering angle and energy loss for the largest total angular momenta. These correspond to the most peripheral, and thereby the most gentle reactions.

The calculated results agree very well with experiment on both the position of the ridge line and the width of the hill perpendicular to the ridge.

The large energy loss component stretches from scattering angle 0° out to around 80°, and is peaked around 300 MeV of energy loss with a quite large dispersion. In the calculated results, this component is due to the more central and intimate reactions, which for this reaction have turned through 0° and come out at negative scattering angles, as illustrated with one example in figure 4. Experimentally, the information from a Wilszinsky plot alone does not allow for determining the sign of the scattering angle. (The falloff of the cross section for very small angles on the calculated plots is due to the tilting of the outgoing reaction plane

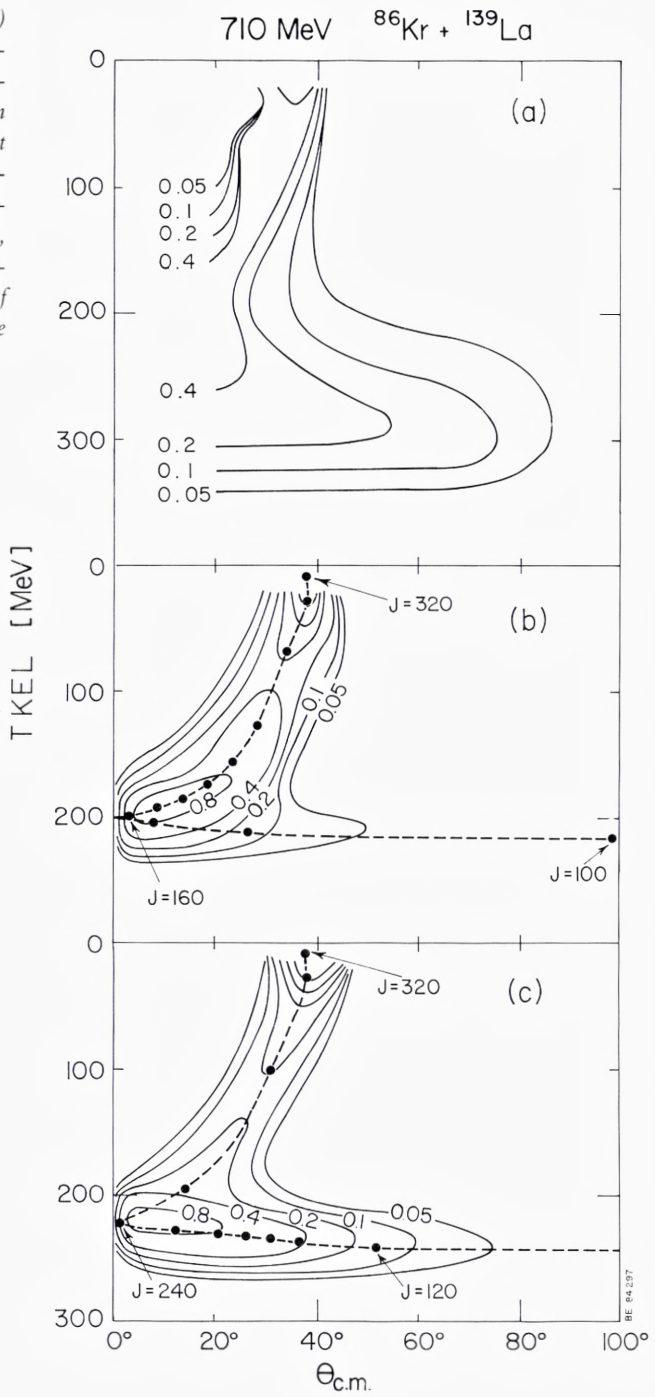

Fig. 3. Experimental, (a) Vandenbosch 1978, and calculated, (b) and (c), Wilszinsky plots for the reaction 710 MeV $^{86}Kr + ^{139}La$. Plot (b) is obtained with the standard prescription for the reduction in the neck damping, while this reduction is removed in the calculation of plot (c). The units for the contours are mb/ (deg×MeV).

relative to the entry reaction plane. The width of the angular range of this falloff is discussed in Døssing 1985c).

The calculated differential cross sections are too much concentrated around the mean trajectory result for the large energy loss component, the dispersion in energy loss for given scattering angle being a factor of two too small. The calculated dispersions agree to within 12% with the estimate (5.4) for the asymptotic value of the variance. Thus, with the mean trajectory implementation, the nucleon exchange transport theory will not be able to account for this aspect of the data.

The average energy loss for this component is around 80 MeV too small in the calculations. This is probably because the description of the shape of the dinuclear system by means of only two parameters, the neck radius and the center separation, does not allow for the elongation of the dinuclear system at the end of the reaction phase, which is needed to loose the extra amount of energy.

The reduction in the wall damping applied in calculation (b) implies that the small energy loss component receives a higher proportion of the cross section than the large energy loss component, whereas the calculation (c) distributes the cross section more evenly on the two components, in better agreement with the data. An intermediate neck damping between the two prescriptions would yield a better agreement than both (b) and (c). The pronounced difference between the two calculations display a sensitivity of the results upon elements of the application of the theory, which have not been consistently studied yet, and this is somewhat discomforting.

6.3 γ ray polarisations

Information on the spin distribution in the two nuclei and on the sign of the scattering angle can be obtained from the polarisation of γ rays emitted from the nuclei during their sequential decay.

The detailed evaluation of the γ ray polarisation on the basis of calculated spin distributions and its relation to the polarisation of the spin in the nuclei is discussed in appendix A.

Figure 4 illustrates how positive and negative scattering angles lead to different senses of rotation in the nuclei. During the reaction the orbital rotation is slowed down, and the average spins in the nuclei after the reaction will point in the same direction as the total angular momentum vector. With the situation depicted in figure 4, the total angular momentum points upwards from the plane of the figure for positive angle scattering and downwards for negative angle scattering. With the coor-

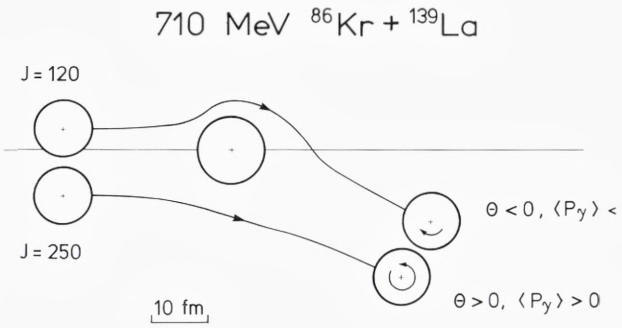

Fig. 4. Calculated trajectories for two values of the total angular momentum for the reaction $^{86}Kr + {}^{139}La$. The two trajectories lead to the same size of the final scattering angle, but with opposite sign. The circular arrows on the outgoing light nuclei show the directions and magnitudes of their average rotation.

dinate system applied, the Y axis points upwards, so a positive scattering angle corresponds to positive polarisations of the spin in both nuclei, and vice versa for negative angles. This sign convention for the polarisation, which is easily remembered, is different from that employed conventionally.

In recent experiments, Schandera 1984, the polarisation of the emitted γ rays has been measured for certain intervals in scattering angle and total kinetic energy loss. Figure 5 shows calculated and experimental polarisations as functions of energy loss for the same reaction as considered in figures 3 and 4. For one interval covering small scattering angles (laboratory scattering angle $11° < \theta_{lab} < 30°$ corresponding to center of mass scattering angle $20° \lesssim \theta_{CM} \lesssim 55°$) three intervals in energy loss were applied, and in addition one interval covered large energy losses and scattering angles ($30° < \theta_{lab} < 68°$, corresponding to $55° \lesssim \theta_{CM} \lesssim 120°$).

The thin graphs in fig. 5 include only partial waves above capture. However, the captured nuclei may separate again, and the thick graphs in fig. 5 include the whole captured part of the cross section, from the highest total angular momentum leading to capture all the way down to zero, assuming that it leads to a separation again of the nuclei.

The angular distribution for the captured and re-separated part is assumed to be uniform, implying that the captured system must have turned a couple of times before separation. As the energy loss is concerned, both the average value and the variance are taken as the values obtained for the smallest total angular momentum not being captured, and the average energy loss is then increased due to the smaller centrifugal energy of the relative motion for the partial waves leading to capture.

The centrifugal energies applied in this small correction are determined by the asymptotic value (4.8) for the orbital angular momentum, inserting the relative moment of inertia for the distance where the nuclei loose contact for the smallest partial wave not being captured. The mean spins in the nuclei emerging after capture and re-emission are likewise derived from the asymptotic values (4.8), but with equal probability of pointing up or down, i.e. with spin polarisation zero, leading to γ ray polarisation zero. For the spin variances, the variances calculated with the smallest partial wave not leading to capture are applied for capture and re-separation.

This is, admittedly, a crude way of including capture and re-emission. It can be regarded as leading to maximal dilution of the polarisation, since the maximal possible cross section for capture and re-separation is included. A more consistent account of capture and re-separation would then most probably lead to results for the polarisation which are between the thick and thin curves in fig. 5.

Figure 6 shows the result of a calculation for the same experiment as shown in fig. 5 but now obtained without the reduction in neck damping, as also applied for part (c) of fig. 3. The large peak around 240 MeV for the cross section for the small angle interval comes from the very pronounced hill in the contour plot (c) of fig. 3.

Calculated polarisations and data for the three other reactions studied in Schandera 1984 are shown in figures 7, 8 and 9.

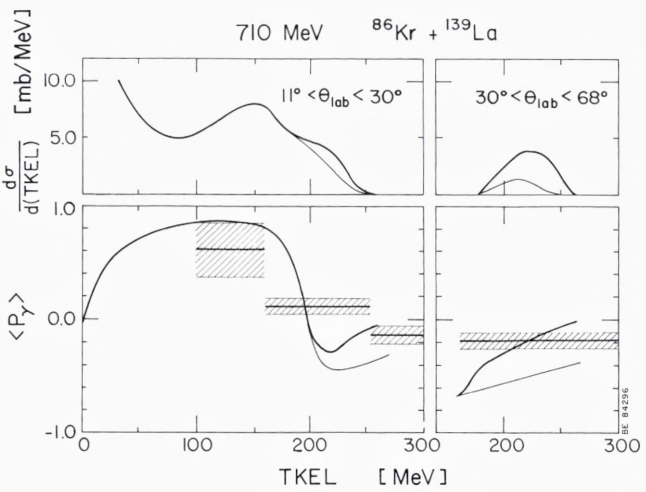

Fig. 5. Calculated and experimental, Schandera 1984, γ ray polarisations for the reaction 710 MeV $^{86}Kr + ^{139}La$. The experimental values are denoted by horizontal lines, covering the energy intervals of averaging applied in the experiments, and the shaded regions show the uncertainties reported. The calculations are performed with the standard implementation of nucleon exchange transport. The thin curves include only the calculated direct cross section, whereas the thich curves also includes capture and re-separation as described in the text.

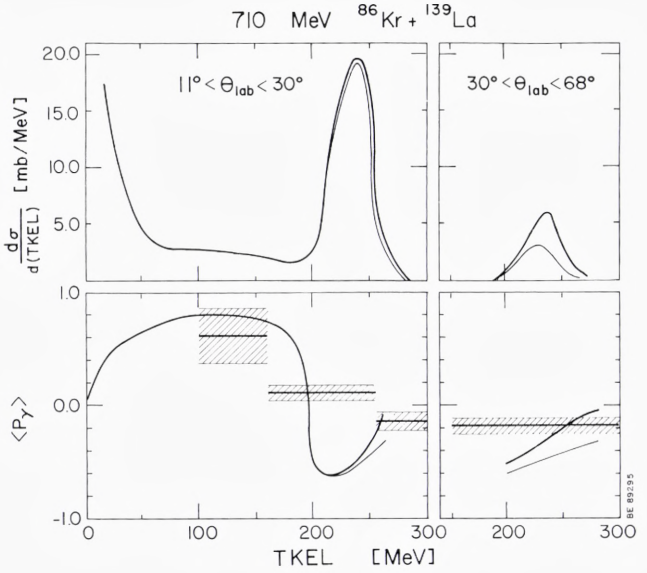

Fig. 6. The same as fig. 5, but now calculated without the reduction in the neck damping, as for part (c) of fig. 3.

6.4. Comparison between calculated and experimental γ ray polarisations.

For all the reactions the interval of the smallest energy losses covered by the experiment is completely dominated by positive angle scattering, and the interval at small scattering angles covers most of the cross section. Thus, the γ ray polarisation for this interval gives fairly direct information about the spin moments, as calculated by solving the equations (4.7) and subsequently transforming to the external coordinate system. For the reactions with ^{139}La as a target, the calculated polarisations are slightly too large when compared to the data for this interval. For the ^{166}Er data, on the other hand, significant discrepancies with the data are apparent.

The energy loss interval in question is centered around half of the maximally calculated energy loss. For this energy loss a generally good agreement with γ ray multiplicity and fission angular distribution data was found in Døssing 1985b. To the extent one can compare the different reactions, we conclude that, except for the reaction 705 MeV ^{86}Kr + ^{166}Er, the γ ray polarisation data are in reasonably good accordance with the other data and with the calculations for intermediate energy losses.

Going to higher energy losses, still within the interval of small scattering angles, the calculated polarisation first decreases weakly because the mean spin vector starts to decrease and the variances grow. However, this decrease is soon overtaken by a much stronger decrease, caused by

the admixture from negative scattering angles. From a certain energy loss, the negative scattering angles dominate. Thus, the polarisation goes steeply through zero, and reaches negative values which can be quite substantial, except for the reaction of 705 MeV ^{86}Kr + ^{166}Er for which the negative scattering angles receive very little cross section according to the present calculation. The decrease in polarisation is also present in

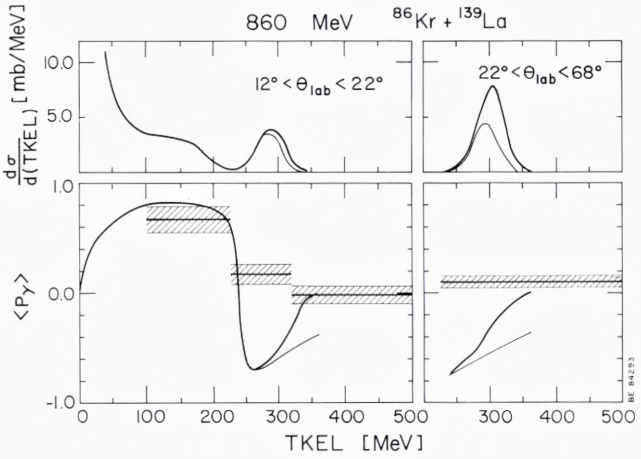

Fig. 7. Same as fig. 5, but for the reaction 860 MeV ^{86}Kr + ^{139}La.

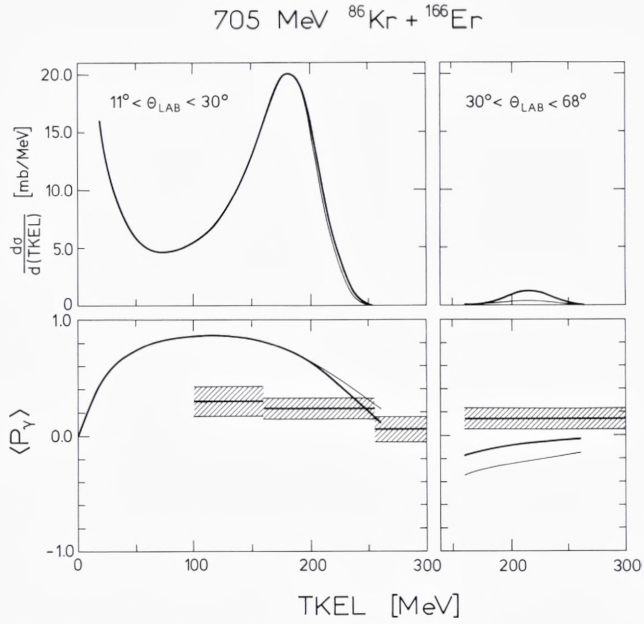

Fig. 8. Same as fig. 5, but for the reaction 705 MeV ^{86}Kr + ^{166}Er.

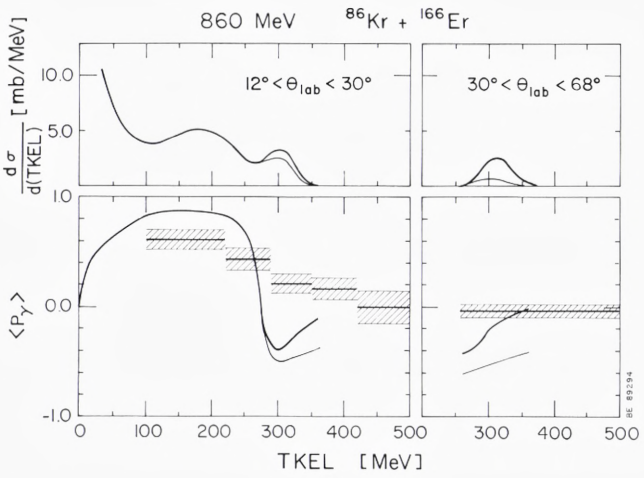

Fig. 9. Same as fig. 5, but for the reaction 860 MeV $^{86}Kr + {}^{166}Er$.

the data, but these display a much smoother behavior than the calculated values. Finally, at the highest energy losses for the small angle interval, the calculated negative values of the γ ray polarsiation are somewhat weakened, because the average spin vector still decreases in size. With inclusion of capture and re-separation, the negative polarisations may be considerably reduced. In the experiments significant negative polarisations are only recorded for one of the reactions at this interval, and the polarisations are generally small.

The comparison to data for the small angle interval for the larger energy losses points in the same direction as the comparison to the Wilszinsky plots, namely that the dispersion in energy loss for given impact parameter is too small. Larger dispersions will mix the positive and negative scattering angles, leading to a smoother behavior of the calculated curves for the polarisation. Also large dispersions in scattering angle for given impact parameter of the order of 40°, which is twice the lower end point of the interval, would explain the data.

The large angle interval only receives contributions from negative angle scattering for the reactions calculated here, and inclusion of capture and re-separation dilutes the polarisation considerably. Without this dilution, the γ ray polarisation is typically calculated to be around –0.5, which tells that the spin dispersions are of approximately the same magnitude as the mean spin vector, cfr. figures A1 and A3. The experimental polarisations are numerically small for this angle interval, and of varying sign. Since both of the two different targets and both of the two bombarding energies display a positive and a neative mean value for the γ ray

polarisation for this angle interval, the only systematic trend seems to be the small values. On the other hand, analysis of fission angular distributions show that the alignment of the spin does not seem to decrease below values of the order of 0.4, Døssing 1985b, even for the largest energy losses. (This is admittedly for other reactions involving heavier targets than the ones discussed here, but the result for the alignment is not expected to be crucially dependent upon whether the target mass is 139 or 208).

The small values of the γ ray polarisation taken together with appreciable spin alignments indicate that in the present reactions both positive and negative scattering angles contribute almost evenly to the cross section for the large energy losses. With the mean trajectory method used here, this will be quite impossible to achieve. For the impact parameters leading to negative scattering angles within this interval, an estimate for the scattering angle dispersion yields 11°, obtained by inserting the values 50×10^{-22} for the reaction time t, 2×10^{-22} for the relaxation time t_{++}, and 2.5 MeV for the effective temperature $\tau^{\star}$ into the expression (5.8). Actually a value of twice the lower end point of the interval, around 100°, is needed. Alternatively, a substantial part of the cross section at these energy losses could correspond to reactions like the capture and reemission discussed here, where the nuclei turn some times before reseparation, thereby averaging the spin polarisation out to small values. Since such a component will have an almost uniform cross section as function of angle, an examination of the Wilszinsky plots will give an upper limit for this component, as discussed in Vandenbosch 1978.

7. Conclusion

The main result of this paper is the application of nucleon exchange transport to calculate Wilszinsky plots and γ ray polarisations. Also, it is demonstrated in the appendix that γ ray polarisations can be quite exactly calculated on the basis of theoretical spin distributions.

Concerning the application of the theory to obtain these results, it is somewhat uncomforting that the results depend so sensitively upon specific details of the implementation, which have not been consistently derived yet. This applies to the prescription for the reduction in the neck damping, and the linear extrapolation of the Coloumb potential for small distances, Randrup 1982.

The comparison of the calculated quantities to data is successful as far

as the small and medium energy losses are concerned. For the larger energy losses, substantial discrepancies between calculated results and data are found. The calculations are not able to account for the large variances in energy loss and scattering angle present in the data for these energy losses. Furthermore, by inspecting the expressions for the variances, it is concluded that variances accumulated during the motion along a mean trajectory will generally be small.

One would expect larger final fluctuations if the fluctuations caused by the nucleon exchange were allowed to couple back on the potentials and form factors for exchange. For example, for motion on the quite flat potential energy surfaces encountered for total angular momenta 100 to 140$\hbar$ for the present reactions, fluctuations in the center separation and the radial momentum may cause substantial dispersions in the reaction time, and thereby in scattering angle. Whether improvements in that direction are enough to obtain significantly better agreement with data is still an open question.

Certainly γ ray polarisations, as investigated in the new experiments, give powerful information and the results are challenging to our understanding of damped nuclear reactions.

It would be valuable if the experiments with the new and powerful set up could be extended to cover also the smallest energy losses, where the polarisation is expected to increase with increasing kinetic energy loss. Also the application to reactions with heavier nuclei would be of interest, since the mixing from negative scattering angles will be minimal, and therefore a more pure information about the spin distribution could be obtained.

Appendix A

This appendix presents a procedure for calculating the average γ ray polarisation starting from a theoretically predicted distribution of spins in a hot nucleus produced in a damped nuclear reaction. The last part shows calculated polarisations for a schematic spin distribution and discusses the information contained in γ ray polarisations and angular distributions of continuum γ rays.

After a damped nuclear reaction the nuclei rapidly dispose of their excitation energy and angular momentum by sequential decay. For light nuclei, often protons and α particles are evaporated, and very heavy nuclei may fission. The relatively neutron rich medium mass nuclei of

interest here evaporate neutrons followed by the emission of γ rays. Only through observation of the decay products can one gain information about the angular momentum.

In this appendix we shall describe the decay with the aim of calculating the average polarisation of the γ rays, as being observed in a polarimeter, Trautmann 1981, taking as a starting point the excited nucleus with a Gaussian distribution of spin variables, as specified by the first and second moments of the spin distribution. This program takes four steps, of which the three last follow the time evolution of the decay: (i) One needs to define the moments of the directional distribution of the spin. (ii) The distribution of the spin magnitude as well as the directional distribution is modified due to neutron evaporation. (iii) A γ ray cascade follows, consisting of statistical γ rays, which cool the nucleus, and yrast type γ rays, which take away angular momentum, but which do not lead to cooling. (iv) The γ rays may scatter on magnetized iron in the polarimeter, and then finally be detected, yielding information about the polarisation.

The average polarisation of γ rays determined in step (iv) is quite closely connected to the average polarisation of the nuclear spin, defined as $\langle S_Y/S \rangle$. We shall in the end of this appendix see how this connection between spin -and γ polarisation depends upon the excitation energy in the nuclei, and the types of γ rays emitted.

Proceeding now with step (i), we first define the moments of the directional distribution, which are the statistical tensor components, Fano 1957. For a given spin distribution function $f(\vec{S})$ in the nucleus it is useful to define for each spin magnitude a normalized directional distribution function, such that $f(\vec{S}) = f_o(S)\, f_s(\hat{S})$. For spins which are large compared to the rank λ, the tensor component of rank λ and magnetic quantum number μ is well approximated by the classical definition as the $\lambda\mu$'th component in an expansion on spherical harmonics:

$$\varrho_{\lambda\mu}(S) = \sqrt{\frac{4\pi}{2\lambda+1}} \langle Y_{\lambda\mu} \rangle_{f_s} \qquad (A.1)$$

$$= \sqrt{\frac{4\pi}{2\lambda+1}} \int f_s(\hat{S})\, Y_{\lambda\mu}(\hat{S})\, d\hat{S}$$

Of special importance for the present discussion are the components with $\mu=0$, which are expansion coefficients on Legendre polynomials:

$$\langle P_{\lambda Y}(S) \rangle \equiv \varrho_{\lambda 0}(S) = \langle P_\lambda \rangle_{f_s} \qquad (A.2)$$

Here the Y in $\langle P_{\lambda Y}\rangle$ denotes that we use the Y axis as polar axis. Extending the average to the whole spin distribution, we can write the two lowest in full:

$$\langle P_Y\rangle = \left\langle \frac{S_Y}{S} \right\rangle \tag{A.3}$$

$$\langle P_{YY}\rangle = \langle P_{2Y}\rangle = \left\langle \frac{3S_Y{}^2 - S^2}{2S^2} \right\rangle$$

$\langle P_Y\rangle$ is called the *polarisation,* and $\langle P_{YY}\rangle$, or $\langle P_{2Y}\rangle$ is called the *alignment* of the spin distribution.

The relations relevant for describing step (ii), the neutron evaporation, are given in Døssing 1985b. Starting at spin S_0 in the original nucleus, the average spin magnitude $\langle S_n\rangle$ after the evaporation of n neutrons is approximately given by

$$\langle S_n\rangle \simeq S_0 \exp\left[-n\left(\tfrac{2}{3}\frac{mR_n^2}{I} + \frac{\hbar^2}{2I\tau_1} - \tfrac{4}{9}\frac{mR_n^2\tau_1}{S_0{}^2}\right)\right] \tag{A.4}$$

The relation between statistical tensors is given by:

$$\varrho_{\lambda\mu}(S_n) = \varrho_{\lambda\mu}(S_0)\left\langle P_\lambda\left(\frac{\vec{S}_0 \cdot \vec{S}_n}{S_0 S_n}\right)\right\rangle \tag{A.5}$$

$$\approx \varrho_{\lambda\mu}(S_0) \exp\left[-n\cdot P'_\lambda(1)\left(\tfrac{4}{9}\frac{mR_n^2\tau_1}{S_0\langle S_n\rangle} + \tfrac{1}{4}\frac{\hbar^2}{S_0\langle S_n\rangle}\right)\right]$$

with the relevant derivatives of the Legendre polynomials

$$P'_1(1) = 1, \quad P'_2(1) = 3, \quad P'_3(1) = 6, \quad P'_4(1) = 10 \tag{A.6}$$

In these relations I is the moment of inertia of the nucleus and $mR^2{}_n$ is the moment of inertia of the neutron at the effective barrier radius R_n. The tempeature τ_1 in the nucleus after the evaporation of the first neutron is given by

$$\tau_1 = \sqrt{\frac{E_0 - \frac{S_0^2}{2I} - B}{a}} \tag{A.7}$$

Here E_0 denotes the excitation energy in the primary nucleus leaving the reaction, B is the average binding energy of the neutrons, and a denotes the level density constant. The average number of neutrons n emitted is

$$n \approx (E_0 - \frac{S_0^2}{2I} - \frac{B}{2})(B + \tfrac{4}{3}\tau_1)^{-1} \tag{A.8}$$

All these relations are derived and discussed in Døssing 1985b, and we apply them together with the parameters for a, I, mR_n^2 and B given in that reference.

Proceeding now with step (iii), the γ ray emission, we can readily generalize the procedure, Døssing 1981, for calculating angular distributions of decay products to include also the polarisation. The polarisation is the helicity of the γ ray, and in Døssing 1981 the helicity representation is applied for the state after the emission.

The probability for emission of decay products in a certain direction determined by polar angles $\theta\varphi$ (relative to the Y-axis) is obtained by applying the projection operator

$$P_{\theta\varphi} = \sum_{h_1 h_2} |h_1 h_2;\theta\varphi\rangle\langle h_1 h_2;\theta\varphi| \tag{A.9}$$

to the density operator after the decay. Letting h_1 denote the helicity of the nucleus after the γ decay, h_2 denotes the helicity of the γ ray, and can take on values 1 or $\div 1$. The projection operator for the emission probability times the average polarisation of the γ ray is then simply

$$P_{\theta\varphi}^{(\mathrm{pol})} = \sum_{h_1 h_2} h_2 \,|\, h_1 h_2;\theta\varphi\rangle\langle h_1 h_2;\theta\varphi| \tag{A.10}$$

Carrying through the same procedure for $P_{\theta\varphi}^{(\mathrm{pol})}$ as for $P_{\theta\varphi}$, one obtains for the emission probability in the direction $\theta\varphi$

$$\begin{aligned} W(\theta\varphi) &= \mathrm{tr}\{P_{\theta\varphi}\,\varrho_S(\text{after decay})\} \\ &= \frac{1}{\sqrt{4\pi}} \sum_{\lambda\mu} A_\lambda(S)\,\varrho_{\lambda\mu}(S)\,Y^*_{\lambda\mu}(\theta,\varphi) \end{aligned} \tag{A.11}$$

and for the emission probability times the average polarisation

$$\begin{aligned} W^{(\mathrm{pol})}(\theta\varphi) &= \mathrm{tr}\{P_{\theta\varphi}^{(\mathrm{pol})}\,\varrho_S(\text{after decay})\} \\ &= \frac{1}{\sqrt{4\pi}} \sum_{\lambda\mu} A_\lambda^{(\mathrm{pol})}(S)\,\varrho_{\lambda\mu}(S)\,Y^*_{\lambda\mu}(\theta,\varphi) \end{aligned} \tag{A.12}$$

In these expressions $A_\lambda(S)$ is the angular distribution coefficient of rank λ. For γ rays $A_\lambda(S)$ has the form:

$$\begin{aligned} A_\lambda(S) = {} & (-)^{S_f - S - \lambda - 1}(2\ell + 1)\sqrt{2S+1} \\ & \times \tfrac{1}{2}(\langle \ell 1 \ell -1|\lambda 0\rangle + \langle \ell -1 \ell 1|\lambda 0\rangle)\, W(\ell S \ell S; S_f \lambda) \end{aligned} \tag{A.13}$$

where ℓ is the multipolarity of the radiation and S_f is the angular momentum of the final state. The sum over the two Clebs-Gordan coefficients in this expression comes from the summation over $h_2 = 1$ and -1 in $P_{\theta\varphi}$. To obtain $A_\lambda^{(\mathrm{pol})}(S)$, $h_2 = 1$ still enters with the plus sign, but the sign for $h_2 = -1$ is inverted, as in the projection operator $P_{\theta\varphi}^{(\mathrm{pol})}$.

Thus $A_\lambda^{(pol)}(S)$ is obtained from $A_\lambda(S)$ by changing this sign:

$$A_\lambda^{(pol)}(S) = (-)^{S_f - S - \lambda - 1}(2\ell + 1)\sqrt{2S+1} \times \tfrac{1}{2}(\langle \ell 1 \ell -1|\lambda 0\rangle - \langle \ell -1 \ell 1|\lambda 0\rangle)\, W(\ell S \ell S; S_f \lambda) \tag{A.14}$$

For all kinds of decay, $A_\lambda(S)$ is zero for odd λ and $A_\lambda^{(pol)}(S)$ is zero for even λ. It is an advantage to change the normalisation of the angular distribution coefficients by defining

$$B_\lambda(S) = \sqrt{2\lambda+1}\,\langle SS\lambda 0|SS\rangle\, A_\lambda(S) \tag{A.15}$$

and equivalently for $B_\lambda^{(pol)}(S)$.

Actually, quite few of these coefficients are needed, since only multipolarity 1 and 2 are emitted in the γ ray cascades, so only coefficients with $\lambda \leq 4$ will be different from zero. For *stretched transitions*, $S_f = S\text{-}\ell$, the coefficients are independent of the size of S, and attain the following values for dipole and quadrupole transitions:

$$\begin{aligned} &\ell = 1: \quad B_0(\ell=1) = 1, \quad B_1^{(pol)}(\ell=1) = \tfrac{3}{2},\ B_2(\ell=1) = \tfrac{1}{2} \\ &\ell = 2: \quad B_0(\ell=2) = 1, \quad B_1^{(pol)}(\ell=2) = 1,\ B_2(\ell=2) = -\tfrac{5}{7}, \\ &\qquad\qquad\qquad\quad B_3^{(pol)}(\ell=2) = -1,\ B_4(\ell=2) = -\tfrac{2}{7} \end{aligned} \tag{A.16}$$

The yrast-type transitions, which make up the bulk of γ transitions are almost exclusively of stretched type. They are preceded by statistical transitions, mainly of multipolarity 1, which are not all stretched. The probability for final spin S_f, $S_f = S-1, S, S+1$ is given by the relative level density at S_f, which is well approximated by the expression:

$$\mathcal{P}(S_f) \quad \alpha \quad \exp\left(-\frac{(S_f - S)S}{\tau_f I}\right) \tag{A.17}$$

where τ_f is a representative temperature for the excitation above the yrast line after emission of a statistical γ ray, and I is the moment of inertia. τ_f is typically around 0.5 MeV. Inserting the B_λ coefficients for $\ell = 1$ and for the different S_f, weighted be the probability factors, one obtains for the average coefficients for statistical transitions:

$$B_0(S) = 1 \tag{A.18}$$

$$B_1^{(pol)}(S)|_{stat} = \frac{\tfrac{3}{2}\exp\left(\frac{S}{\tau_f I}\right) + 0 - \tfrac{3}{2}\exp\left(-\frac{S}{\tau_f I}\right)}{\exp\left(\frac{S}{\tau_f I}\right) + 1 + \exp\left(-\frac{S}{\tau_f I}\right)}$$

$$= \tfrac{3}{2}\sinh\left(\frac{S}{\tau_f I}\right)\left(\cosh\left(\frac{S}{\tau_f I}\right) + \tfrac{1}{2}\right)^{-1}$$

$$B_2(S)|_{stat} = \frac{\frac{1}{2}\exp\left(\frac{S}{\tau_f I}\right) - 1 + \frac{1}{2}\exp\left(-\frac{S}{\tau_f I}\right)}{\exp\left(\frac{S}{\tau_f I}\right) + 1 + \exp\left(\frac{S}{\tau_f I}\right)}$$

$$= \left(\cosh\left(\frac{S}{\tau_f I}\right) - 1\right)\left(2\cosh\left(\frac{S}{\tau_f I}\right) + 1\right)^{-1}$$

Here it is assumed that S and S_f are much larger than 1, otherwise some of the angular distribution coefficients become quite complicated functions of S and S_f. For small S, the coefficients $B_1^{(pol)}$ and B_2 for statistical γ rays are close to zero anyway, so it would be quite superfluous to insert the more exact values. As standard values for the paramenters τ_f and the number, N_{stat} of statistical γ rays, we take the temperature 3 MeV above the yrast line for the nucleus in question, and 3 statistical γ rays per nucleus i.e.

$$\tau_f = \sqrt{\frac{3}{a}} \qquad \mathcal{N}_{stat} = 3 \qquad a = \frac{A}{10} \tag{A.19}$$

where A is the mass number.

With these definitions, we can now define an effective angular distribution coefficient for the whole γ ray cascade. By p_1 and p_2 we denote the fraction of stretched yrast type γ rays of multipolarity $\ell=1$ and 2, respectively. The average number of $\ell=1$ and 2 transitions and the average number of γ rays as function of the spin S_0 are then given by

$$\mathcal{N}_{\ell=1}(S_0) = p_1\frac{\langle S_n\rangle}{p_1+2p_2}, \quad \mathcal{N}_{\ell=2}(S_0) = p_2\frac{\langle S_n\rangle}{p_1+2p_2},$$

$$\mathcal{N}_\gamma(S_0) = \mathcal{N}_{\ell=1}(S_0) + \mathcal{N}_{\ell=2}(S_0) + \mathcal{N}_{stat} \tag{A.20}$$

where $\langle S_n\rangle$ is the average spin (A.4) in the nucleus after neutron emission. Including the dilution factors (A.5) for the statistical tensors, the effective angular distribution coefficient as function of S_0 is given by

$$\mathcal{B}_\lambda(S_0) = \left\langle P_\lambda\left(\frac{\vec{S}_0\cdot\overleftarrow{S}_n}{S_0S_n}\right)\right\rangle \times \left[\mathcal{N}_{\ell=1}(S_0)\, B_\lambda(\ell=1)\right. \tag{A.21}$$

$$\left. + \mathcal{N}_{\ell=2}(S_0)\, B_\lambda(\ell=2) + \mathcal{N}_{stat} B_\lambda(\langle S_n\rangle)|_{stat}\right] / \mathcal{N}_\gamma(S_0)$$

and equivalently for $\mathcal{B}_\lambda^{(pol)}(S_0)$ for the odd λ.

The angular distribution can be written as

$$4\pi\,\mathcal{W}(\theta,\varphi) = C_0 + C_2\,P_2(\cos\theta) + C_{22}\sin^2\theta\cos 2\varphi + C_4\,P_4(\cos\theta) + C_{42}(7\cos^2\theta-1)\sin^2\theta\cos 2\varphi + C_{44}\sin^4\theta\cos 4\varphi \tag{A.22}$$

with the coefficients for $\mu=0$ given by

$$C_\lambda = \int f(\vec{S})\,\mathcal{N}_\gamma(S)\,\mathcal{B}_\lambda(S)P_\lambda\left(\frac{S_\gamma}{S}\right)\mathrm{d}\vec{S} \tag{A.23}$$

Likewise the angular distribution, mulitplied by the average polarisation, can be written as

$$4\pi\,\mathcal{W}^{(\mathrm{pol})}(\theta,\varphi) = C_1^{(\mathrm{pol})}\,P_1(\cos\theta) + C_3^{(\mathrm{pol})}P_3(\cos\theta) + C_{32}^{(\mathrm{pol})}\cos\theta\sin^2\theta\cos 2\varphi \tag{A.24}$$

with the coefficients for $\mu=0$ given by

$$C_\lambda^{(\mathrm{pol})} = \int f(\vec{S})\,\mathcal{N}_\gamma(S)\,\mathcal{B}_\lambda^{(\mathrm{pol})}(S)P_\lambda\left(\frac{S_\gamma}{S}\right)\mathrm{d}\vec{S} \tag{A.25}$$

We now turn to step (iv), to calculate the γ ray polarisation, as it will be determined by the polarimeter. The γ ray polarisation is calculated by integrating the angular distributions (A.22) and (A.24) without and with inclusion of the polarisation over the angular range covered by the polarimeter, weighted by the transmission function $\frac{\mathrm{dT}}{\mathrm{d}\Omega}(\theta)$ and by the sensitivity function A (θ):

$$\langle P_\gamma\rangle = \frac{\int_{\theta_1}^{\theta_2}\int_0^{2\pi}\mathcal{W}^{(\mathrm{pol})}(\theta,\varphi)\,\frac{A(\theta)}{\langle A\rangle}\,\frac{\mathrm{dT}}{\mathrm{d}\Omega}(\theta)\,\mathrm{d}\varphi\,\sin\theta\mathrm{d}\theta}{\int_{\theta_1}^{\theta_2}\int_0^{2\pi}\mathcal{W}(\theta,\varphi)\,\frac{\mathrm{dT}}{\mathrm{d}\Omega}(\theta)\,\mathrm{d}\varphi\,\sin\theta\mathrm{d}\theta} \tag{A.26}$$

The functions for the forward scattering polarimeter applied in the experiments under discussion here are evaluated and discussed in Trautmann 1981, and they are quite well approximated by:

$$A(\theta) \quad \alpha \quad \text{constant} \tag{A.27}$$

$$\frac{\mathrm{dT}}{\mathrm{d}\Omega}(\theta) \quad \alpha \quad \sin^{-2}\theta$$

Since the polarimeter is symmetric around the reaction normal, the terms containing cos2φ and cos4φ in (A.22) and (A.24) integrate out to zero. Applying the functions (A.27) and integrating over the angular

range $20° < \theta < 45°$ covered by the polarimeter, the following result is obtained in terms of the expansion coefficients (A.23) and (A.25):

$$\langle P_\gamma \rangle = \frac{0.850\ C_1^{(pol)} + 0.290\ C_3^{(pol)}}{C_0 + 0.591\ C_2 + 0.016\ C_4} \tag{A.28}$$

In this procedure, the dependence of the functions $A(\theta)$ and $\frac{dT}{d\Omega}(\theta)$ on the energy of the γ ray energy has been neglected. Below 500 keV of γ ray energy, these functions become very small, and this will hinder the detection of some of the yrast type γ rays, especially those of multipolarity $\ell=1$.

In the remainder of this appendix we shall discuss results of calculated polarisations, applying a distribution function of the spin with equal variances in all directions:

$$f(\vec{S}) = (2\pi\sigma)^{-3/2} \exp\left(-\frac{(\vec{S} - \langle S_Y \rangle \hat{Y})^2}{2\sigma^2}\right) \tag{A.29}$$

where $\hat{Y}$ is a unit vector along the reaction normal.

It is convenient to plot the results as function of the spin polarisation $\langle P_Y \rangle$ (A.3). The magnitudes of the mean spin vector and the dispersion are shown as function of the polarisation in figure A1. Applying a specific parametrisation like (A.29) the higher order statistical tensors become funtions of the polarisation. These functions are shown in figure A2. For most values of the spin polarisation, the higher order tensors are substantially smaller than the polarisation.

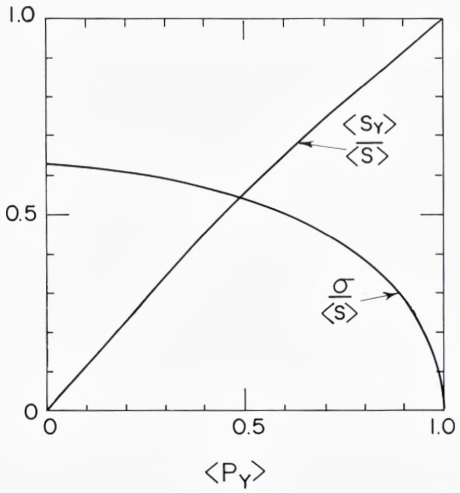

Fig. A1. Sizes of the average spin vector and the standard deviation of the spin distribution along all coordinates for the Gaussian parametrisation applied to illustrate the γ ray polarisation results, shown as function of the average spin polarisation.

Fig. A2. Sizes of higher order tensors as function of the spin polarisation for the Gaussian parametrisation.

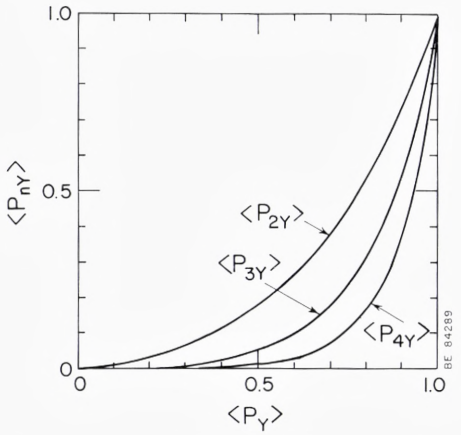

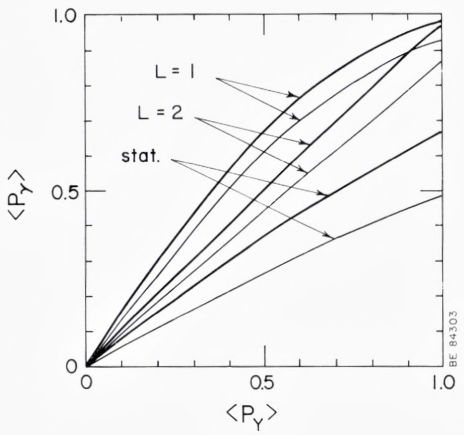

Fig. A3. γ ray polarisation as function of spin polarisation for the three different kinds of γ rays contributing to the cascade. The average spin size is 30 units, and the parameters applied describe the decay of a nucleus with a mass number around 160 and excitation energy of 200 MeV. The effects of neutron evaporation are included in the thin curves and left out for the thick curves.

Figure A3 shows calculated γ ray polarisations as function of the spin polarisation. They are calculated separately for each of the three different kinds of γ rays contibuting to the cascade, stretched dipole, stretched quadrupole, and statistical transitions. The parameters are determined for a nucleus of mass number 160, excitation energy 200 MeV, and average spin magnitude 30ħ. The figure addresses the same question as figure 7 of Trautmann 1981, and the thick curves for the stretched transitions are very similar to the results presented in that figure. They are obtained by completely neglecting the effects of neutron evaporation. Neutron evaporation from the quite high excitation energy of 200 MeV is included in the results shown by the thin lines, and one can see that the decrease in polarisation and higher order tensors caused by the neutrons really changes the γ ray polarisation.

Figure A4 shows the calculated γ ray polarisation for an yrast composition of 90% quadrupole and 10% dipole transitions. This composition we adopt as standard. In figure A4 neutrons are fully included, and the average spin magnitude varies between the different curves. One can see that the spin magnitude has quite some influence upon the results. For the cases we shall deal with in section 6, the average spin magnitude is around $30\bar{}$, and the excitation energy is around 80 MeV. The γ ray polarisation for these cases will be typically 10% smaller than the spin polarisation, in qualitative agreement with the results shown on fig. A4.

Fig. A4. Same as fig. A3, but for different average spin sizes, and with inclusion of the effects of neutrons. The yrast part of the cascade is assumed to consist of 10% stretched multipolarity 1 transitions and 90% stretched multipolarity 2 transitions, and the number of statistical transitions included is 3 per cascade.

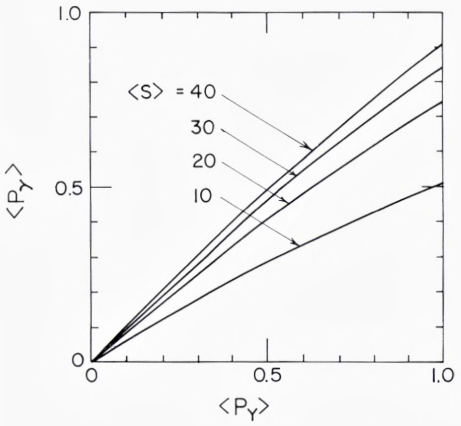

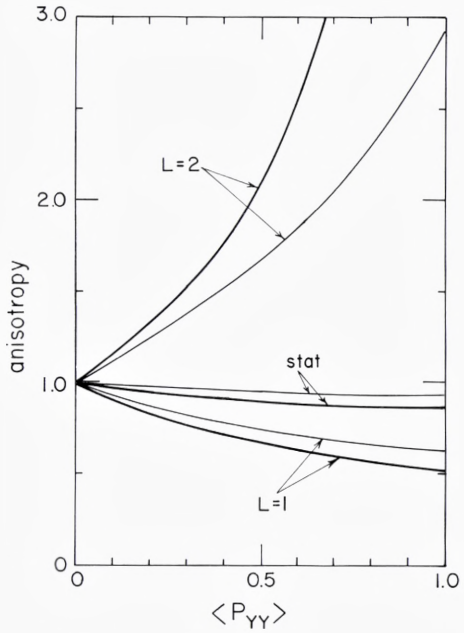

Fig. A5. Anisotropy as function of spin alignment for the three different kinds of γ rays contributing to the cascade. The parameters are the same as for fig. A3.

The results shown in figure A4 do not depend crucially upon the composition of the yrast type γ rays, because the most important polarisation angular distribution coefficient $B_1^{(pol)}$ (A.16) has the same sign and a similar magnitude for stretched dipole and quadrupole transitions. This similarity is also apparent in figure A3.

In contrast to this situation, we show in figure A5 for each of the three kinds of γ rays the anisotropy af the angular distribution, which can be written in terms of the coefficients for the angular distribution (A.22):

$$\text{anisotropy} = \frac{\frac{1}{2\pi}\int W(\theta=\frac{\pi}{2}, \varphi)d\varphi}{W(0,\varphi)} = \frac{C_0 - \frac{1}{2}C_2 + \frac{3}{8}C_4}{C_0 + C_2 + C_4} \qquad \text{(A.30)}$$

In figure A5, the result is plotted as function of the alignment, since the polarisation does not enter, but otherwise the parameters are identical to those used for figure A3. Since the anisotropy has opposite signs for dipole and quadrupole γ rays (due to the opposite signs of the B_2 angular distribution coefficents (A.16)), the angular distribution of continuum γ rays is a problematic tool to study the spin alignment, because the result will depend crucially upon the multipolarity composition of the yrast type γ rays.

ACKNOWLEDGEMENTS. *The author is grateful to Thomas B. Thriges Fond for the award of the fellowship. Numerous stimulating discussions with Jørgen Randrup during the course of this work are gratefully acknowledged.*

References

Agassi 1978: D. Agassi, C. M. Ko and H. A. Weidenmüller, Phys. Rev. **C18** (1978) 223

Ayik 1976: S. Ayik, B. Schürmann and W. Nörenberg, Z. Phys. **A277** (1976) 299, **A279** (1976) 145

Balian 1984: R. Balian, P. Bonche, H. Flocard and M. Veneroni, Nucl. Phys. **A428** (1984), 79 c, and references therein

Barrett 1978: B. R. Barrett, S. Shlomo and H. A. Weidenmüller, Phys. Rev. **C17** (1978) 544

Blocki 1978: J. Blocki, Y. Boneh, J. R. Nix, J. Randrup, M. Robel, A. J. Sierk and W. J. Swiatecki, Ann. Phys. **113** (1978) 330

Britt 1982: H. C. Britt, H. Erkkila, A. Gavron, Y. Patin, R. H. Stokes, M. P. Webb, P. R. Christensen, O. Hansen, S. Pontoppidan, F. Videbaek, R. L. Ferguson, F. Plasil, G. R. Young and J. Randrup, Phys. Rev. **26C** (1982) 1999

Broglia 1981: R. A. Broglia, C. H. Dasso and A. Winther, in Proceedings of The International School of Physics »Enrico Fermi«, held in Varenna, Italy, july 9-21 1979, editors R. A. Broglia, R. A. Ricci and C. H. Dasso. (North Holland 1981)

Dasso 1979: C. H. Dasso, T. Døssing and H. C. Pauli, Z. Phys. **A289** (1979) 395

Davies 1978: K. T. R. Davies, V. Maruhn-Rezwani, S. E. Koonin and J. W. Negele, Phys. Rev. Lett. **41** (1978) 632

Davies 1981: K. T. R. Davies and S. E. Koonin. Phys. Rev. **C23** (1981) 2042

Døssing 1981: T. Døssing, Nucl. Phys. **A357** (1981) 488

Døssing 1985a: T. Døssing and J. Randrup. Nucl. Phys. **A433** (1985) 215

Døssing 1985b: T. Døssing and J. Randrup. Nucl. Phys. **A433** (1985) 280

Døssing 1985c: T. Døssing and J. Randrup. submitted to Physics Letters (1985)

Esbensen 1978: H. Esbensen, A. Winther, R. A. Broglia and C. H. Dasso, Phys. Rev. Lett. **41** (1978) 296

Fano 1957: U. Fano. Rev. Mod. Phys. **29** (1957) 74, and references therein

Feldmeier 1984: H. Feldmeier and H. Spangenberger, preprint. GSI Darmstadt (1984)

Ko 1979: C. M. Ko, Phys. Lett. **81B** (1979) 299

Köhler 1979: H. S. Köhler and H. Flocard, Nucl. Phys. **A323** (1979) 189

Martinot 1984: M. Martinot, C. Ngo and F. Lepage (editors), Proceedings of the International Conference on Theoretical Approaches of Heavy Ion Reaction Mechanisms, Paris may 14-18 1984, published as volume **428** of Nucl. Phys. (1984)

Moretto 1980: L. G. Moretto and R. P. Schmidt. Phys. Rev. **C21** (1980) 204

Moretto 1984: L. G. Moretto, in Proceedings of The International School of Physics »Enrico Fermi«, held in Varenna, Italy, july 9-august 6 1982, editors L. G. Moretto and R. A. Ricci (North Holland 1984)

Nix 1965: J. R. Nix and W. J. Swiatecki, Nucl. Phys. **71** (1965) 1

Nörenberg 1975: W. Nörenberg, Z. Phys. **A274** (1975) 241

Nörenberg 1982: in »Nuclear Physics«, proceedings of the Workshop held at I. C. T. P., Trieste, Italy, 5-30 october 1980, editors C. H. Dasso, R. A. Broglia and A. Winther, (North Holland 1982)

Randrup 1979: J. Randrup, Nucl. Phys **A327** (1979) 490

Randrup 1982: J. Randrup, Nucl. Phys. **A383** (1982) 468

Schandera 1984: C. Schandera, Ch. Lauterbach, J. de Boer, W. Dünnweber and W. Trautmann, preprint, Sektion Physik, Universitat Munchen (1984), to be published in Nukleonika

Schmidt 1982: R. P. Schmidt and A. J. Pacheco, Nucl. Phys. **A379** (1982) 313

Schröder 1981: W. U. Schröder, J. R. Huizenga and J. Randrup, Phys. Lett. **98B** (1981) 355

Shlomo 1979: S. Shlomo, B. R. Barrett and H. A. Weidenmüller, Phys. Rev. **C20** (1979) 1

Tang 1981: H. H. K. Tang, C. H. Dasso, H. Esbensen, R. A. Broglia and A. Winther, Phys. Lett. **101B** (1981) 10

Trautmann 1981: W. Trautmann, C. Lauterbach, J. de Boer, W. Dünnweber, C. Graw, W. Hamann, W. Hering and H. Puchta, Nucl. Inst. Meth. **184** (1981) 449

Vandenbosch 1978: R. Vandenbosch, M. P. Webb. P. Dyer, R. J. Puigh and R. Weisfield, Phys. Rev. **C17** (1978) 1672

Weidenmüller 1980: H. A. Weidenmüller, in Prog. Part. and Nucl. Phys. vol 3. editor D. Wilkinson. (Pergamon Press 1980)

Wolschin 1978: G. Wolschin and W. Nörenberg, Phys. Rev. Lett. **41** (1978) 691

Wolschin 1981: G. Wolschin, in Proceedings of The International School of Physics »Enrico Fermi«, held in Varenna, Italy, july 9-21 1979, editors R. A. Broglia, R. A. Ricci and C. H. Dasso. (North Holland 1981).